

Review

Not peer-reviewed version

Solution Combustion Synthesis for various Applications: A Review of the Mixed Fuel Approach

Samantha Padayatchee , [Halliru Ibrahim](#) * , [Holger B Friedrich](#) , Ezra J Olivier , [Pinkie Ntola](#)

Posted Date: 28 February 2025

doi: [10.20944/preprints202502.2330.v1](https://doi.org/10.20944/preprints202502.2330.v1)

Keywords: solution combustion synthesis; decomposition rate, mixed fuels; nanomaterial; morphology; physicochemical



Preprints.org is a free multidisciplinary platform providing preprint service that is dedicated to making early versions of research outputs permanently available and citable. Preprints posted at Preprints.org appear in Web of Science, Crossref, Google Scholar, Scilit, Europe PMC.

Copyright: This open access article is published under a Creative Commons CC BY 4.0 license, which permit the free download, distribution, and reuse, provided that the author and preprint are cited in any reuse.

Disclaimer/Publisher's Note: The statements, opinions, and data contained in all publications are solely those of the individual author(s) and contributor(s) and not of MDPI and/or the editor(s). MDPI and/or the editor(s) disclaim responsibility for any injury to people or property resulting from any ideas, methods, instructions, or products referred to in the content.

Review

Solution Combustion Synthesis for Various Applications: A Review of the Mixed Fuel Approach

Samantha Padayatchee ¹, Halliru Ibrahim ^{1,*}, Holger B Friedrich ², Ezra J Olivier ³
and Pinkie Ntola ¹

¹ Department of Chemistry, Durban University of Technology, P.O Box 1334, Durban, 4000, South Africa

² School of Chemistry and Physics, University of KwaZulu-Natal, Private Bag X54001, Durban, 4000, South Africa

³ Centre for HRTEM, Physics Department, Nelson Mandela University, Port Elizabeth, South Africa

* Correspondence: hallirui@dut.ac.za, +27723431791 (H.I.)

Abstract: As Solution Combustion Synthesis (SCS) becomes a universal route to metal oxide nanomaterials, so does it pave way for mixed fuel combustion synthesis as an advance approach to the synthesis of materials of desirable properties for diverse applications. Major significance is attached to the rates of decomposition and combustion temperatures of the fuel as determinant factors of the morphology and physicochemical properties of the materials obtained. This has promoted the use of mixed fuel systems characterized by lower decomposition temperatures of organic fuels and higher rates of combustion. The review work presented herein provides a comprehensive analysis of the applications of mixed fuel SCS in ceramics, recycling of lithium battery materials, fuel cells and nanocomposite materials, while taking into consideration the effects of the mixed fuel system on the physicochemical and morphological properties of those materials. as compared to their analogues prepared via single fuel SCS.

Keywords: solution combustion synthesis; decomposition rate, mixed fuels; nanomaterial; morphology; physicochemical

1. Introduction

Part of the attractiveness of green chemistry is that it is based on a set of principles that reduces or eliminates the use or generation of hazardous substances in the design, manufacture, and application of chemical products [1]. The combined use of such chemical principles led to rapid development of the green chemistry framework that takes into consideration economically viable processes and environmentally benign products. The solution combustion synthesis (SCS) is a versatile method for the production of material powders for diverse applications [2]. It is a green chemistry approach that is gaining wide acceptance as a viable and cost effective substitute for the initial approaches to the bulk production of metal oxide nanostructured materials, and is now a workhorse technique in materials science [3–6]. The ease of implementation, high-throughput, the versatility of chemistries, and capacity for the production of high-surface area powders are among the success recorded with the SCS approach and make it an outstanding technique among its contemporaries [7]. The technique is relatively novel in its content and various modes of applications. The design and preparation methods play a prime role in determining the structural, surface characteristics and unique properties for the desired application of the final products [8].

The redox reaction between suitable oxidizer (usually metal nitrates), and an appropriate organic fuel (i.e. sucrose, urea, citric acid, glycine or hydrazide) is highly favoured towards the formation of desired products in SCS. Deganello et al. summarized the process of SCS into three steps i.e. formation of the combustion mixture, formation of the gel and then the combustion of the gel [6]. These steps are achieved at a gradient temperature range of 80 °C to >200 °C (Figure 1), and are characterized by solvent evaporation to combustible gases, self-ignition and combustion.



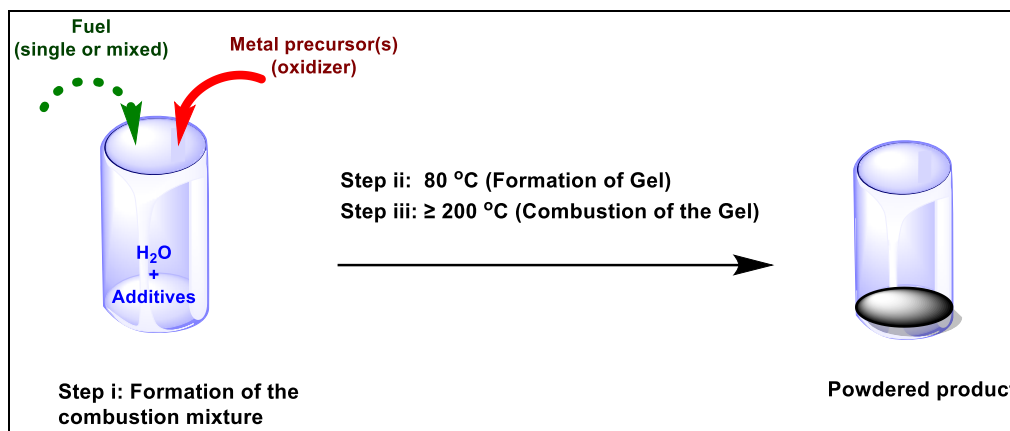


Figure 1. Illustration of three main steps in solution combustion synthesis.

Most products of SCS are fabricated metal oxides that are of great technological importance in advanced materials for energy generation [9], catalysis [10,11], ceramics [12,13], fuel and solar cells [5,14], batteries, super capacitors, optics [4,15], metal recycling, and photocatalytic [16] and environmental applications [6,17]. So far, the SCS route has been employed to produce a large variety of solid materials such as metals, sulphides, carbides, nitrides and single or complex metal oxides, metal-doped materials and alloys [18–22]. Despite all these advantages, the SCS is not free of shortcomings that can somewhat limit its applications.

A recent review by Novistkaya et al.[3] has shed light on such issues arising from the use of the SCS technique, like powder agglomeration, less control on powder morphologies, and the presence of leftover organic impurities from the associated incomplete combustion. A variety of factors including the type of fuel, fuel-to-oxidizer ratio, mixture of fuels, amount of water, pH and combustion temperature, as well as the presence of additives are identified as responsible for such deviations in morphological and physicochemical properties of the resultant material [11,23]. The nature, quantity and/or mixture of the fuel used in any SCS plays a central role in the optimization of the material properties. This is because the fuel plays the central roles of a reducer during the combustion of the mixture/formation of the gel substance, a chelating agent and a microstructural template [5,6,24]. It is then typical of a fuel for SCS to comprise of chelating functionalities can that prevent precipitation of metal ions and help preserve the compositional homogeneity of all the constituents via the formation of strong coordinate bonds [6,18].

There is a wealth of literature and reviews on the use of single fuels for various applications [18,21,25]. Several studies suggest that the combination of various fuels can potentially be more effective than using a single fuel in terms of good control of adiabatic combustion temperature of the reaction mixture, the type and number of gaseous products released and other related factors [5,6,25]. However, there is no published review that comprehensively discusses the usage of the mixed fuel approach. This review, hence, intends to provide a holistic perspective of the use of mixed fuel solution combustion synthetic approach in various applications. The study provides a comprehensive discussion on the positive influence of the mixed fuel on the morphological and physicochemical parameters of the product materials. Consequently, this work provides prospects in the fine adjustment of the mixed fuel SCS approach for the development of more efficient materials for energy and environmental applications.

2. The Mixed Fuel Solution Combustion Synthesis Approach

The role of fuel in influencing the final powder properties with regards to the microstructure and morphology has been extensively studied [18,26–29]. Based on these studies, fuels are classified with reference to the prevailing functional group on the chemical structure of the compound. Thus, amino, carboxylic, hydroxyl, and multifunctional are the four recognized categories of fuels [6,30]. Some common organic molecules which fall within the categories of fuels in SCS are citric acid

(C₆H₈O₇), dextrose (C₆H₁₂O₆), glycine (C₂H₅NO₂), sucrose (C₁₂H₂₂O₁₁), urea (CH₄N₂O) and hydrazine hydrate (N₂H₄. H₂O).

In this regard, the use of mixed fuel SCS has shown unique control over the physicochemical properties of the synthesized materials [6,26,27]. This is due to the influence of mixed fuel system in improving the performance of the combustion and hence the nature of the products, which cannot be obtained via the single fuel SCS [31]. Material properties such as surface area, particle size distribution, and agglomeration are easily and conveniently fine-tuned by the mixed fuel system. Typically, the solution combustion reaction occurs by an exothermic reaction of flammable gases (such as NO_x, NH₃, CO, etc.) that originate from the decomposition of the starting materials (i.e. oxidisers and fuels) [32]. Hence, the combustion behaviour is dependent on the amount and nature of these gases, which can then be tuned by fuel type [23,26,33]. Various fuel mixtures can be used based on factors such as the fuel's chemical structure and chelating ability of the fuel. Other key factors include the ability of the fuel to act as a microstructural template, and the role of a fuel's reducing valency in regulating the maximum temperature and heating rate of a reaction [23]. Notable examples of such mixed fuel systems employed in SCS for a specific target material are presented in Table 1.

Table 1. Common mixed fuels systems and target materials in SCS.

Entry	Fuel mixture	Material	Reference
1	Urea+ β -alanine	Ca ₃ Al ₂ O ₆ powders	[34]
2	Urea and glycine	SrAl ₂ O ₄ powders	[35]
3	Urea and glycine	ZnAl ₂ O ₄ powders	[4]
4	Urea and glycine		
5	Urea, glycine and starch	MgAl ₂ O ₄ powders	[36]
6	Citric and oxalic acid	LaAlO ₃ powders	[37]
7	Urea and ammonium acetate	Al ₂ O ₃ -ZrO ₂ nanocomposite	[38]
8	Urea and glycine	Fe ₃ O ₄ powders	[39]
9	CTAB and citric acid	Fe ₃ O ₄ powders	[40]
10	Glycine and citric acid	ZnO powders	[41]
11	CTAB and glycine	ZnO powders	[16]
12	Urea and glycine	CeO ₂ -CeAlO ₃ nanocomposites	[42]
13	Succinic and citric acid	Bio-ceramic calcium phosphates	[43]
14	Urea and sucrose	Sr-doped lanthanum manganite	[26]
15	Citric acid, cellulose, sucrose polyethylene glycol	Sr and Fe- doped barium cobaltite	[5]
16	Urea and glycine	Ni _{0.5} Zn _{0.5} Fe ₂ O ₄ nanoparticles	[44]
17	Glycine and CTAB	BiFeO ₃ powders	[31]
18	Urea and glycine	γ - Alumina	[27]
19	CTAB and glycine	CoFe ₂ O ₄	[45]
20	Urea and glycine	Gd ₃ Al ₂ Ga ₃ O ₁₂ :Ce ³⁺ -Cr ³	[28]
CTAB = Cetyltrimethylammonium bromide			

On this basis, a higher specific surface area and smaller particles size in a SrFeO₃- δ catalysts for the reduction of nitrobenzene was achieved by Naveenkumar et al.[46] through the use of mixed citric acid, glycine and oxalic acid fuels (Table 1, entry 2). Similarly, (α , β)-SrAl₂O₄ powders were

reported to be directly formed by using a mixture of urea and glycine fuels in work by Ianos et al.[35]. This contrasts with their failed initial attempt in the use of single fuel (urea or glycine) to synthesize the SrAl_2O_4 . The failure due to the use of single fuel in the combustion synthesis is attributed to the low amount of energy released during the combustion process [8]. On the other hand, the direct formation of (α , β)- SrAl_2O_4 powders in the mixed fuel approach was ascribed to the enhanced combustion performance of mixed fuel via a very substantial increase of released gases, resulting in the spontaneous ignition to a flaming combustion reaction [6,8].

Research findings have shown that glycerine combined with urea, or any other amino mixed fuel is best suited for the synthesis of bimetallic materials (Table 1, entries 1–5). Combustion reactions that result in the synthesis of metallic oxide materials are usually carried out with mixed fuels based on citric acid with Cetyltrimethylammonium bromide (CTAB) or glycine or a mixture of the latter two fuels (Table 1). This might be due to the combustion rate of CTAB or glycine which is beneficial for anisotropic growth of the products [16,47]. Where a heavy metal doped material is targeted in the SCS; a poly mixed fuel system, as reported for Sr and Fe- doped barium cobaltite, is applied [5]. These approaches have been successfully employed in the synthesis of materials for various applications, including optics, the battery industry, ceramics, nanocomposites, fuel cells and pigments.

3. Application of Mixed Fuels SCS in the Preparation of Desirable Nanomaterials

3.1. Ceramics

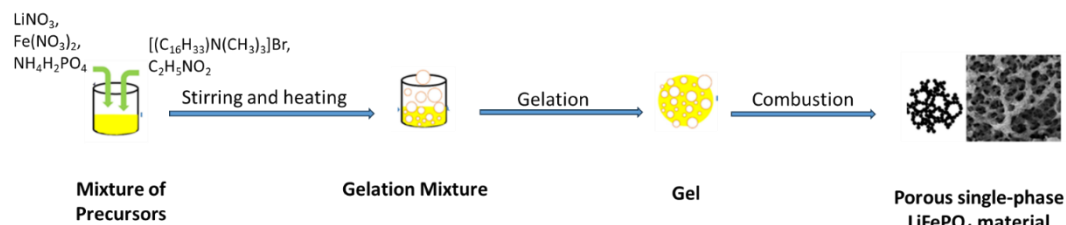
It is essential to understand that the fine-tuning of crystallite and particle sizes via combustion parameters contributes to desired material characteristics, thereby making mixed fuel SCS a versatile method for modifying ceramics to meet specific application requirements [12,43]. The control over the crystal structure of the ceramic material mitigates agglomeration and ensures uniform particle distribution during formation, thereby expediting the standardization of the mechanical and thermal properties of the ceramic materials [21]. A study conducted by Lin et al. on the fabrication and evaluation of γ - LiAlO_2 ceramic materials; identified a highly promising material for use in tritium-breeding applications [48]. The mechanical strength of these breeding blanket ceramics assumes a vital role in maintaining material stability [49] which is significant, particularly, in relation to the rate efficiency at which tritium is released and recovered. In this vein, comprehensive evaluation of the morphology, mechanical properties, and electrical characteristics of γ - LiAlO_2 ceramics under a variety of conditions was done using the mixed fuel SCS approach.

In another development, the preparation of γ - LiAlO_2 involved the use of a glycine/urea/leucine-nitrate combinations [50]. An aqueous solution comprising glycine and urea, or glycine and leucine in conjunction with metal nitrates, served as the components (mixed fuel and metal precursor respectively) for the synthesis of the ceramic. The simultaneous thermal analysis (STA) of precursors obtained under conditions of fuel and oxidizer stoichiometry, showed the presence of impurities attributed to incomplete decomposition of initial salts containing carbon fragments of fuel and nitrate groups. An exception was the precursor from the dual-fuel SCS reaction, φ (glycine : urea) = 1 : 3, in which pure γ - LiAlO_2 powder was formed. Particle morphology, phase analysis, and particle size analysis confirmed that a highly reactive pure γ - LiAlO_2 with characteristic fine crystalline texture was successfully synthesized. However, the replacement of lithium nitrate with lithium carbonate was found to allow one to reduce the process temperature and the relative amount of organic fuel. As a result, the content of carbon fragments in the product significantly decreased after synthesis. Under these specific conditions, the γ - LiAlO_2 ceramics displayed a consistent microstructure, increased conductivity of the lithium metal, and superior bending strength in comparison to synthesized materials from other fuel mixtures/ratios. These properties aligned with the intended outcomes of the mixed fuel approach [27]. Remarkably, both the lithium-rich ceramics and those with lithium-deficient phases demonstrated improved ionic conductivities, although it is probable that the mechanisms driving these enhancements are different [48,51].

3.2. Lithium Batteries

The mixed fuel approach in the SCS of battery materials is pivotal for achieving high specific discharge capacity and excellent capacity retention [52]. The control offered by SCS on the physicochemical properties of the material allows for optimize ion transport, enhanced reactivity, and ensures uniform distribution in the battery materials, with exceptional electrochemical performance for efficient energy storage [9,53].

The phase evolution occurring in the mixed CTAB and glycine fuel during SCS of hierarchical porous LiFePO₄ powders was found to be dependent on the nature of the intermediate phases [54]. Thus, the combustion synthesis using an appropriate amount of the mixed fuels followed by calcination of the precursors at 700 °C (Scheme 1), led to the production of highly crystalline single-phase LiFePO₄ electrode materials with a high specific discharge capacity and capacity retention [54]. The structural and microstructural properties of the powders, including crystallinity, specific surface area, and particle size, were found to be crucial factors in determining their electrochemical performance [55]. The hierarchical porous microstructure and small particle size of the powders are beneficial for the electrode kinetics [56,57], leading to improved desired properties in terms of charge/discharge capabilities. Additionally, the porous microstructure and small particle size were found to benefit the electrode kinetics, as indicated by electrochemical spectroscopy [58].

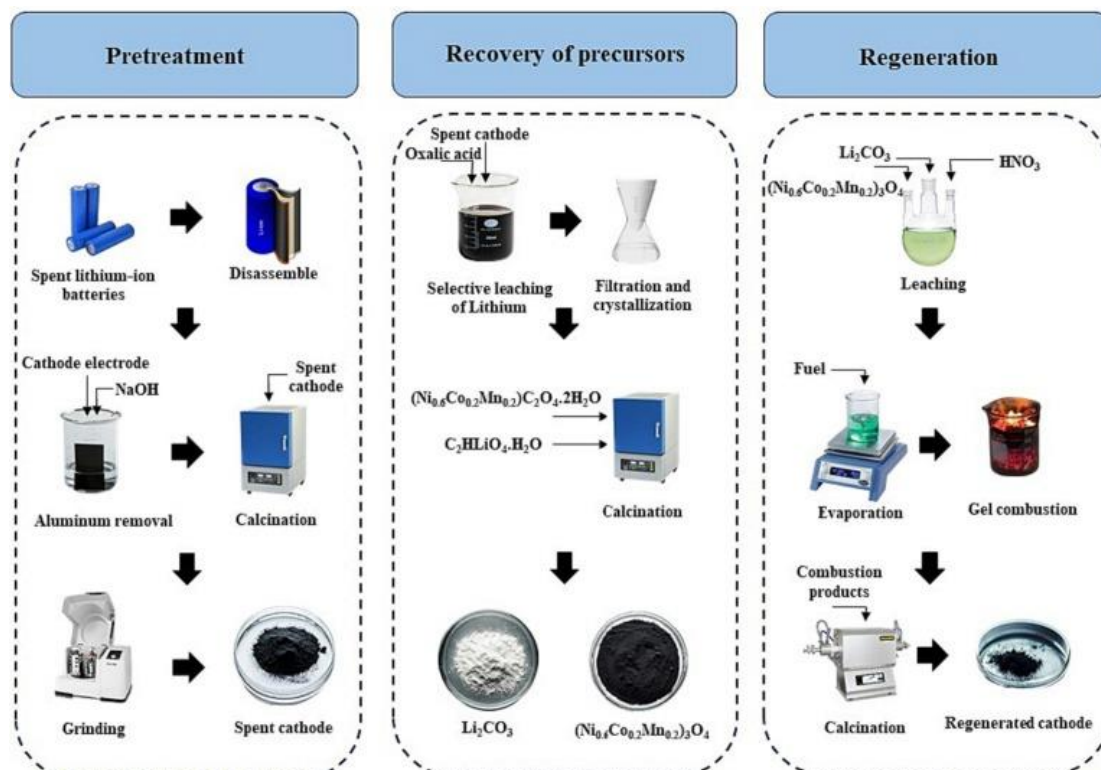


Scheme 1. Preparation of single-phase LiFePO₄ electrode materials by mixed fuel SCS [54].

In a recent and sustainable development, the use of mixed fuel SCS as a recycling approach for spent Lithium-ion Batteries (LIBs) has become a subject of interest to material scientists. The approach has eased the high cost of materials, low yield due to degradation of materials, risk of environmental contamination and other challenges posed with the use of either the open-loop [59] or the chemical synthetic[7,60] recycling approaches of the cathode material from the leachate of spent LIBs. This recycling approach, which is based on a self- propagating high-temperature process; offers a simple, flexible, low-cost, and high-yielding method for the preparation of the cathode materials of LIBs. Suitable organic fuels for regenerating cathode materials in the SCS include urea, citric acid, and glycine. The pretreatment and recovery process involves the dissolution into the leachate of spent cathode material, after which the precursor solution is gelled and ignited by increasing the prevailing temperature [61]. While burning the organic fuel; the heat and gaseous products are liberated during the combustion reaction, providing the required thermal energy for crystallization of the final products with spongy and foamy microstructure [62].

Mahanipour et al. regenerated a cathode material with high specific surface area and porous morphology (Scheme 2) from mixed fuel SCS of spent LIBs [9]. At the beginning, the spent cells were soaked in 10% (w/v) brine solution for the removal of residual electric charge, and then manually disassembled to allows physical separation of the cathode electrodes. These are then pulverized into particulate forms and treated with aqueous NaOH solution (2.5 M, pulp density of 100 g/L) at ambient temperature for 2 h to remove the Al current collector and electrolyte. Burning of the pretreated materials at 650 °C for 4 h allowed for the successive removal of organic solvent and binder. The recovery of the lithium content in the cathode material was selectively achieved by leaching with oxalic acid. Separation of the leached mixture gave a lithium oxalate solution (C₂HLiO₄.H₂O) as the filtrate, while the residue consisted of the dihydrate triplex nickel-cobalt-manganese oxalate (Ni_{0.6}Co_{0.2}Mn_{0.2})C₂O₄.2H₂O). The removal of all volatiles by heating the filtrate at 600 °C for 5 h

crystallized out the lithium carbonate, while the other residual triplex metal oxalate was oxidized to the corresponding oxide by calcination at 650 °C for 4 h under aerobic conditions [51]. Both recovered materials were then transformed to the nitrate precursors by dissolving in 2 M HNO₃ with vigorous stirring at high temperature. The resulting solution was then used in the SCS approach by treatment with citric acid, CTAB, polyvinylpyrrolidone (PVP), and a mixture of CTAB and PVP fuels, in a fuel to metal precursor molar ratio of 4:1. The combustion reaction by the various organic fuels was monitored and the ignition behaviour of the respective gel formed from each set of the fuel mixture was observed (Scheme 2). The afforded combusted products were successively crushed and calcined at 480 °C for 5 h in air atmosphere and then heat-treated at 750 °C for 15 h under oxygen atmosphere to yield the regenerated LiNi_{0.6}Co_{0.2}Mn_{0.2}O₂ cathode powders from the spent LiBs.



Scheme 2. Descriptive illustration of steps involved in the regeneration of cathode materials from spent LiBs. Reprinted with permission from Mahanipour et al.[9].

The structural, microstructural, and electrochemical properties of the regenerated LiNi_{0.6}Co_{0.2}Mn_{0.2}O₂ cathode powders are assumed to be influenced by the fuel type or mixture involved in the SC recycling. The slow combustion reaction rate of mixed CTAB-PVP fuels led to the better layered crystal structure of the regenerated cathode materials. Furthermore, the liberation of a large amount of gaseous products is attributed for the porous structure with high specific surface area in the synthesized material by using a mixture of CTAB and PVP fuels. The CTAB-PVP as-synthesized powders were found to have higher electro-chemical performance, including a high discharge specific capacity of 155.9 mAh g⁻¹ at 0.1 C and a high-capacity retention rate of 94 % following 100 charging/discharging cycles at a current rate of 0.5 C [9]. The outcomes showed that the mixed fuel SCS method is a facile and simple route for regenerating the cathode materials from the spent LIBs with high crystal quality and good electrochemical properties.

3.3. Pigments

Precise control of stoichiometry is essential for a pigment spinel material as it forms its cubic Fd-3m crystal structure. In this context, Chamani et al. employed various fuel mixtures for the SCS to evaluate the characteristic structural and physicochemical impact on CoCr₂O₄ ceramic pigment

nanoparticles [63]. Mixtures of the fuels including ethylenediamine/oxalic acid (En/Ox), ethylenediamine/citric acid (En/Cit), oxalic acid/citric acid (Ox/Cit), and a triplex mixture of ethylenediamine, oxalic acid, and citric acid (En/Ox/Cit); resulted in the production of greenish-blue cobalt chromite ceramic pigments. However, the synthesized materials from En/Cit and En/Ox/Cit mixed fuels exhibited higher purity, smaller crystallite size and lower degree agglomeration when compared to those from other fuel mixtures.

The synthetic route for the CoCr_2O_4 ceramic pigment nanoparticles followed a general pattern where the mixture of the aqueous solutions of the stoichiometric amounts of metal nitrates and fuel were first made in the reaction vessel [64]. The resulting mixture was homogenized by vigorous stirring at 90 °C for 2 h. Subsequent increase in the heating temperature to 300 °C resulted in the self-ignition of the solution in the reaction vessel. The ignition reaction occurred spontaneously with characteristic release of a significant amount of gases and formation of a fluffy foamy sample. The reaction temperature was maintained at 300 °C to allow for complete combustion. The final synthesized material was then obtained after calcination at 600 °C for 3 h.

Analysis of the morphological properties of the synthesized pigment materials showed that the utilization of Cit, Ox/Cit, En/Cit, and En/Ox/Cit fuels leads to the formation of CoCr_2O_4 spinel nanoparticles (Table 2, entries 4 – 7). In contrast, the use of both non-stoichiometric and stoichiometric En/Ox mixed fuels fails to produce pure CoCr_2O_4 spinel (Table 2, entries 1 – 3). It is then worth noting that the choice of fuel types significantly influences both the enthalpy of combustion and the resulting adiabatic flame temperature. The highest adiabatic temperatures were recorded for as-synthesized samples from entries 6 and 7 in Table 2. The calculated adiabatic temperatures reveal that the Ox/Cit and En/Ox/Cit fuel combinations yield the lowest and highest adiabatic temperatures, respectively. Furthermore, summarized data in Table 2 on the Field-Emission Scanning Electron Microscopy (FESEM) and Energy Dispersive X-ray (EDX) analyses of the as-synthesized samples from entries 1 and 2 show the broadest particle size distribution and hence, the highest degree of agglomeration [63]. On the other hand, the as-synthesized samples from entries 6 and 7 displayed the narrowest particle size distribution and, of course, the lowest degree of agglomeration [65]. Additionally, the EDX data revealed that the molar ratio of Cr to Co is approximately 2 for entries 4 – 7; signifying the presence of a pure CoCr_2O_4 spinel phase. Further analyses of the synthesized materials' colour properties with the CIELab colourimetric system, and comparison with values obtained with the reference standard CoCr_2O_4 revealed that the parameter attribute a^* of the as-synthesized samples from entries 6 and 7 (in Table 2), are significantly more negative than what has been previously reported for analogous as-synthesized pigment from single fuel SCS [66,67]. This suggests that the intensity of the green color in the as-synthesized samples 6 and 7 is notably higher. Moreover, the L^* values for as-synthesized samples 6 and 7 are lower, suggesting that these samples possess a deeper and darker green hue. In general, the as-synthesized CoCr_2O_4 pigment materials (Table 2; entries 6 and 7) have the smallest particle size distribution, and offer better dark green color applications when compared to their previously reported analogues [67]. The analyzed properties further reinforce that the En/Cit and En/Ox/Cit mixed fuels SCS produce spinel nanoparticles that exhibit the desired properties which are only attainable via the mixed fuel approach.

Table 2. Effect of mixed fuel SCS approach on the morphology of as-synthesized CoCr_2O_4 ceramic pigment nanoparticles [63].

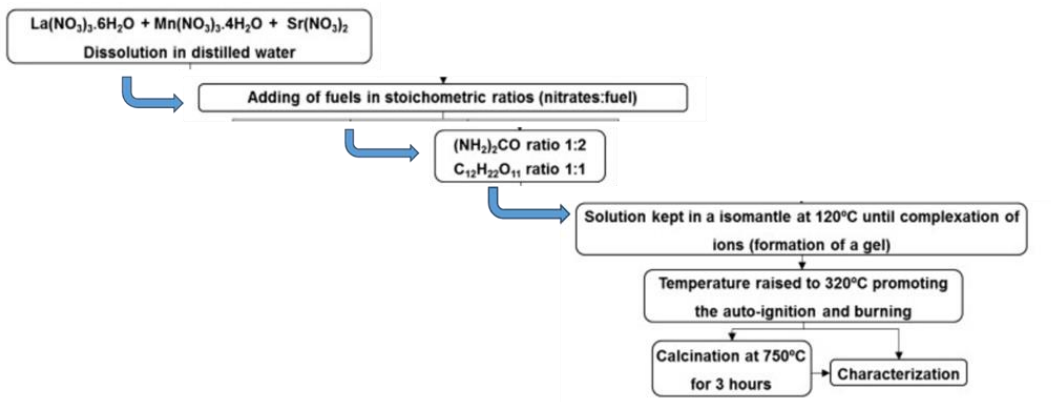
Entry	Mixed fuel	Particle size (nm)	Morphology	Agglomeration n	Atomic ratio (Cr : Co)	Adiabatic temp/°C
1	En/Ox	50-350	Rod shaped	Very high	0.004	-
2	En/Ox(excess)	50-150	Rod shaped	Very high	0.14	-
3	En(excess)/Ox	10-30	Rod shaped	Low	1.78	-

4	Cit	10-30	Cubic	Low	2.13	1262.65
5	Ox /Cit	35-80	Cubic	Low	2.3	1141.47
6	En/Cit	10-25	Cubic	Very low	2.26	1411.83
7	En/Ox Cit	10-25	Cubic	Very low	2.26	1839.93

The mixed fuel SCS approach in pigment preparation profoundly influences critical properties in the material product. Precise stoichiometry control forms the cubic $Fd\cdot3m$ crystal structure, essential for spinel materials. The combustion process mitigates agglomeration, ensuring uniform dispersion and optimal colour, while fine-tuning crystallite and particle size customizes the optical attributes of the material. This approach enables high-purity, and tailored compositions for diverse colour applications. In this intricate interplay, solution combustion synthesis with the mixed fuel approach crafts pigments that meet specific colour and optical criteria.

3.4. Fuel Cells

To improve the performance of Solid Oxide Fuel Cell (SOFC) cathodes, it is crucial to design the final microstructure in a way that promotes efficient gas flow and maximizes the availability of reactive sites [68,69]. In this regard, novel fuel mixtures comprising of urea and sucrose at different ratios were investigated for the synthesis of Lanthanum Strontium Manganite (LSM) perovskite, with particular emphasis on the powder's morphology [26]. The fuel systems featuring both urea and sucrose were mixed in the precursor solution, in a reducers-to-oxidizers stoichiometric ratio of 1:2 for the fuel urea and 1:1 for the fuel sucrose. Both fuel systems resulted in the formation of LSM orthorhombic perovskite, which after calcination at 750 °C yielded the corresponding rhombohedral perovskite $La_{0.9}Sr_{0.1}MnO_3$ powder (Scheme 3). The comparisons of the characterization results from the synthesized samples with those from the CS of either single fuel indicate that the incorporation of sucrose in the precursor solution in conjunction with urea, ensued in an increase in the specific surface area on the synthesized rhombohedral perovskite [26]. The mixed fuel system modified the agglomerates microstructure which tend to form a wide interconnected sub micrometric porous structure, while the single use of sucrose led to the formation of very sparse agglomerate with extremely thin microstructure [26]. This facilitates gas flow and enhances the reactivity of the cathode materials in the former [14,70].



Scheme 3. Isolated flow chart for the mixed fuel SCS of Lanthanum Strontium Manganite (LSM) perovskite [26].

3.5. Nanocomposites

Low oxidation state metal compounds, such as metal nitrates and chlorides, are chosen for their solubility and reduction capabilities in the formation of nanoparticles for various applications [71]. The phases that emerge during the synthesis determine the eventual structure; often consisting of nanoparticles or nanocrystals embedded within a matrix material. The mixed fuel SCS approach, which is characterized by the combination of two or more fuels and an oxidizer, provides fine-tuned

control over the synthesis, influencing nanoparticle formation and, of course the matrix material's composition and structure [33]. In a related study conducted by Aruna et al.[72] stable low oxidation state nano-composites of CeO_2 - CeAlO_3 powders were produced using the solution combustion method. The study utilized two distinct fuel combinations viz: (a) solely urea and (b) a combination of urea and glycine, in conjunction with the respective metal nitrates as precursors. When urea was used as the only fuel, the resultant product comprised of a nano-crystalline CeO_2 phase, while Al_2O_3 was present in an amorphous state. On the other hand, when the mixture of the fuels was employed, a combination of nano-sized CeO_2 and CeAlO_3 phases was obtained.

The use of a mixture of fuels thus favoured the formation of CeAlO_3 and gave in smaller crystallites, leading to enhanced sintering capabilities as compared to the products obtained from the combustion of a single fuel (urea). Characterization of the samples from either fuel systems using images from Transmission Electron Microscopy (TEM) revealed that particles of the sample prepared with the mixed fuel displayed a well-packed microstructure composing of a narrow size distribution, with an average size of approximately 10 nanometers (Figure 2; b). In contrast, the particles of the sample obtained from using solely urea as fuel exhibited a connected but porous network of larger grains (Figure 2; a). Similarly, the Selected Area Electron Diffraction (SAED) pattern obtained from the solely urea synthesized sample is consistent with its X-ray diffraction result and all the observed diffraction rings index to the CeO_2 phase (Figure 2; a). However, the corresponding SAED pattern due to the sample synthesized from a combination of urea and glycine (Figure 2; b) showed rings due to both CeAlO_3 and CeO_2 . All the observed rings are easily indexed to either of the phases. Though there exists overlap of the two phases, the appearance of some rings exclusive to each of the phases (i.e. rings shown for CeO_2 at (1 1 1) and (0 2 4), while for CeAlO_3 at (1 1 1)) [72], confirmed that the synthesized sample from the mixed fuel approach is indeed a nano-composite of CeAlO_3 and CeO_2 .

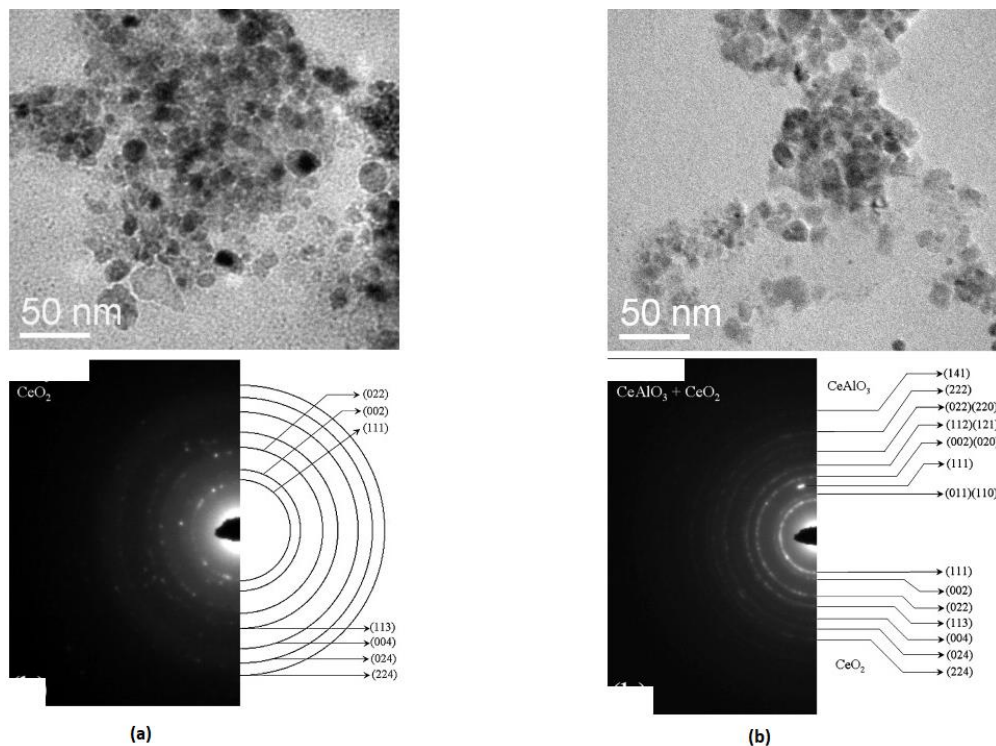


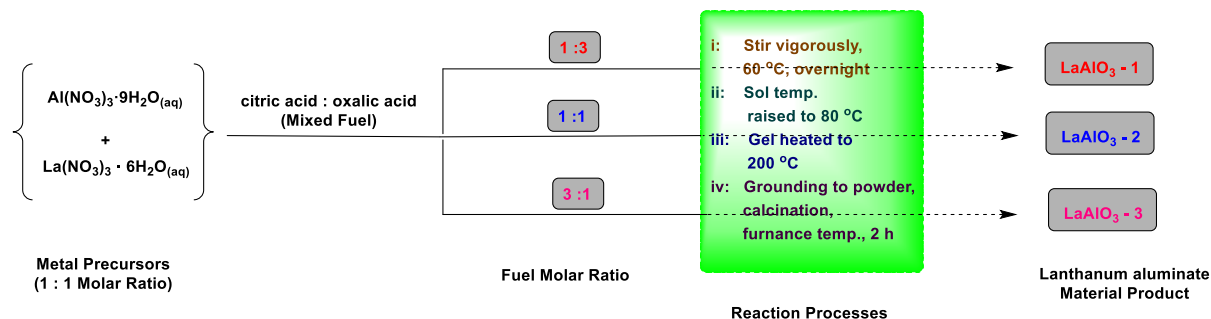
Figure 2. TEM images (top) and SAED rings patterns (bottom) for (a) the synthesized sample prepared from solely urea, and (b) the synthesized sample prepared from mixed fuel of urea and glycine. Reprinted with permission [72].

The smaller crystallite sizes achieved in the mixed fuel synthesized sample contribute to improved sintering compared to the solely urea sample, which has relatively larger particles. This difference in microstructure of the sintered pellets directly explains the observed variation in the

densities of the sintered materials. The combustion synthesis method using a mixture of fuels is, hence suggested as a viable route to stabilize low oxidation state compounds, such as CeAlO_3 , which are highly desirable for the development of nanocomposites. This approach can enhance the sintering process and lead to the formation of materials with improved properties and characteristics.

3.6. Dielectrics

Lanthanum aluminate (LaAlO_3), known for its perovskite-type structure [73], has gained significant attention due to its diverse range of applications, including its utility in dielectric resonators [74,75]. The traditional solid-state reaction process for the synthesis of the LaAlO_3 perovskite presents inherent challenges, such as the need for high reaction temperatures, the formation of large crystallite sizes, limited chemical uniformity, and poor sintering properties [76–78]. To address these issues, a new approach that employs the use of a mixed fuel system of citric acid and oxalic acid as fuel source along with the corresponding metal nitrates was used to successfully produced nanosized LaAlO_3 powders [37]. The synthesis involved the initial mixing of a 1:1 molar ratio of aqueous solutions of the metal precursors. The mix for the fuel systems is to have a total fuel concentration of 0.01 M. This allows for the synthesized samples to be described based on the molar ratios of the mixed fuel. Hence, lanthanum aluminate samples; LaAlO_3 -1, LaAlO_3 -2 and LaAlO_3 -3 were prepared using mixtures of citric acid and oxalic acid in the molar ratios of 1:3, 1:1 and 3:1 respectively. In each instance, the mixed fuels were added to a La-Al (1:1 molar) aqueous solution and stirred vigorously, while keeping the initial fuel/oxidant molar ratio in the reaction mixture at unity. The resultant sol was continuously stirred for several hours at constant temperature of 60 °C until it turned into a yellowish sol, after which the temperature is rapidly raised to 80 °C (Scheme 4). This led to visible changes in the viscosity and colour of the sol as it turns into a transparent thick gel. Further heating at elevated temperature of 200 °C for 2 h turned the gel into a fluffy, polymeric citrate precursor, which was then ground into powder, and calcined at varying furnace temperatures for 2 h to yield the corresponding lanthanum aluminate samples.



Scheme 4. Preparation of the Lanthanum aluminate perovskites by the mixed fuel SCS at varying molar ratios of citric acid and oxalic acid fuels [37].

The rate of crystallization of the aluminate samples is influenced by the prevailing temperature and the heating schedule. The X-ray diffraction (XRD) results highlight the significant influence of the fuel mixture ratio on the crystallite size of the synthesized powders. Samples calcined at 700 °C gave a broad continuum XRD pattern (Figure 3; i) characteristic of an amorphous sample. Those calcined at 750 °C or 800 °C, gave XRD patterns (Figure 3; ii, iii) confirming the presence of rhombohedral LaAlO_3 with a perovskite structure [37]. Specifically, the calculated crystallite sizes for LaAlO_3 -1, LaAlO_3 -2, and LaAlO_3 -3 were 23.6, 32.2, and 26.8 nm, respectively. These measurements were made for samples calcined at 750 °C, and are quite significant when compared to those reported using single fuel systems of citric acid, oxalic acid or tartaric acid [24]. In a related development, a suite of pure LaAlO_3 nanoparticles prepared from a citrate precursor was reported to have an average range of crystallite sizes of 29 – 35 nm [79].

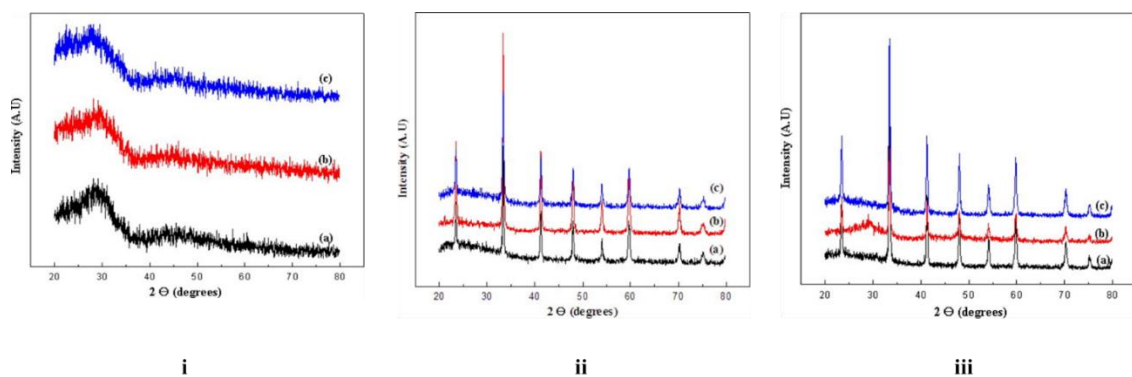


Figure 3. XRD patterns of lanthanum aluminate as-synthesized powders prepared from the molar ratios of mixed citric acid/oxalic fuel mixtures: (a) LaAlO_3 -1; (b) LaAlO_3 -2; (c) LaAlO_3 -3 and calcined at respective temperatures of: i- $700\text{ }^\circ\text{C}$; ii- $750\text{ }^\circ\text{C}$; iii- $800\text{ }^\circ\text{C}$. Reprinted with permission [37].

It's worth noting that the choice of a mixture of fuels (citric acid and oxalic acid) facilitated a reduction in crystallite size when compared to the product obtained with a single fuel system. Furthermore, the ratio of the fuel mixture significantly influenced the morphology and size of the resulting powders. LaAlO_3 -1, prepared using a citric acid : oxalic acid (1 : 3 molar ratio), exhibits the smallest crystallite size of 23.6 nm. This correlates with the average particle size of approximately 41 nm for LaAlO_3 -1, as determined by Transmission Electron Microscopy (TEM). In contrast, the particles of both LaAlO_3 -2 and LaAlO_3 -3 displayed considerable aggregation [37]. Thus, it can be concluded that the utilization of a mixture of fuels not only reduces the exothermicity of the combustion reaction but can also significantly reduce the crystallite size [3,80].

3.7. Optics

The specific material phases generated through mixed fuel solution combustion synthesis exert a profound influence on the resultant material's band gap and emissions, thus bearing direct relevance to its optical properties [81]. These multifaceted influences stem from the interplay of various factors such as crystal structure, phase purity, dopants and defects, quantum confinement effects, and the composition of the synthesized material [15]. Studies on zinc aluminate spinel (ZnAl_2O_4), have garnered significant attention due to its wide range of applications in sensors, ultraviolet (UV) photo electronic devices, and as catalyst support [4,82,83]. This interest is driven by the unique characteristics of the nanostructured ZnAl_2O_4 powders, which consist of a broad band gap of approximately 3.8 eV, high fluorescence efficiency, strong chemical and thermal stability, and low surface acidity [84]. In this vein, the mixed fuel SCS offers the best route to producing zinc aluminate spinel with optimum desirable properties for the various optical applications. The recent work by Mirbagheri et al. utilized a set of molar ratios of urea-glycine mixed fuels for the combustion synthesis of Zinc aluminate spinel [4]. The resulting powders were subjected to morphological characterization, specific surface area measurement, and optical property determination. The findings from the analyses revealed that nearly single-phase ZnAl_2O_4 powders are obtainable after calcination at $700\text{ }^\circ\text{C}$ for the synthesized sample procured in a closed system, whereas intermediate phases are still detectable in some open and closed systems calcined at $600\text{ }^\circ\text{C}$ (Figure 4) [4].

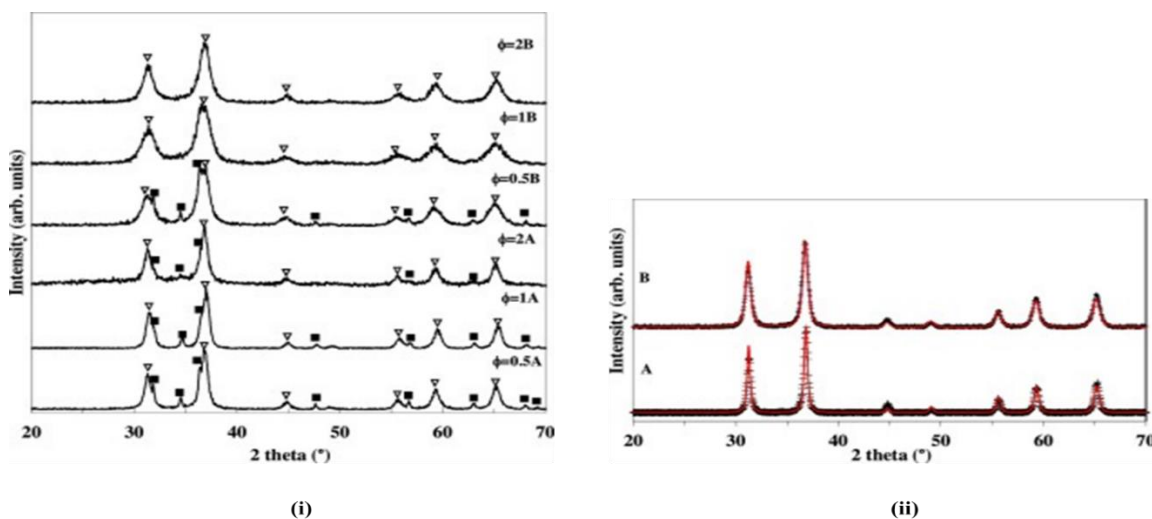
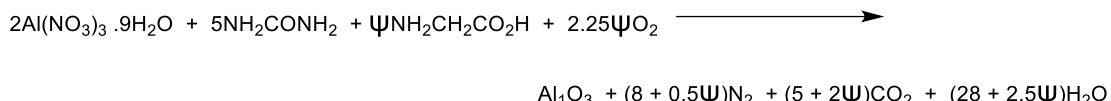


Figure 4. (i) XRD patterns of the calcined powders at 600 °C in open (A) and closed (B) systems at various fuel contents (■: ZnO and ▼: ZnAl₂O₄). (ii) XRD patterns and Rietveld refinement results of the calcined powders after calcination at 700 °C and prepared by open (A) and closed (B) system at ϕ value of 2. Reprinted with permission [4].

The properties of the synthesized zinc aluminate powder are also influenced by the mixed fuel to oxidant ratio (ϕ). Notably, ZnAl₂O₄ powders synthesized at a ϕ value of 0.5 contained both ZnAl₂O₄ and ZnO phases (Figure 4). The presence of ZnO in the sample via the open system decreased with an increase in the ϕ value to 2 and resulted in nearly single-phase ZnAl₂O₄ powders similar to those obtained using the closed system approach (Figure 4; i). The reflections due to the ZnO phase in the open system are easily removed with calcination at 700 °C, while powders prepared by the closed system need a lower calcination temperature for complete formation of the spinel phase (Figure 4). The higher calcination temperature required by powders prepared via the open system approach is attributed to the segregation of intermediate phases formed during the combustion reaction [85]. Furthermore, the existence of the ZnAl₂O₄ as combustion product prior to calcination in the open system, gave rise to larger crystallite size ZnAl₂O₄ powders when compared to those produced from the closed system. The ZnAl₂O₄ powders synthesized via the closed system displayed a nearly normal spinel structure, where Zn²⁺ cations predominantly occupied tetrahedral sites and Al³⁺ cations were situated in octahedral sites [86]. This normal spinel structure resulted in the absence of blue emissions in the range of 400–500 nm [4,87]. In contrast, the powders prepared in the open system exhibited a smaller band gap energy, measuring 3.52 eV, in comparison to the closed system, which had a band gap energy of 3.90 eV [4].

3.8. Catalyst Supports

The mixed urea and glycine fuel SCS of γ -alumina has proven to be a versatile method for engineering superior catalytic materials [27]. Nanocrystalline γ -alumina - a polymorph of alumina characterized by small crystalline size has major applications in catalysis and as a support material due to its remarkable attributes like a high surface area and porosity [88,89]. Sherikar et al. initiated research that involved altering the exothermic redox reaction between aluminum nitrate nonahydrate [Al(NO₃)₃·9H₂O] and urea [CO(NH₂)₂] by using a fuel mixture in the combustion synthesis [27]. In this setup, CO(NH₂)₂ served as the stoichiometric fuel, and glycine (C₂H₅NO₂) was added as excess fuel. The composition of the fuel mixture was designed so that the amount of urea remained constant under stoichiometric conditions, while glycine was added in multiples of 10 weight percentages, ranging from 0 to 40w% of the urea content to afford five sample compositions that were made with notation U00G, U10G, U20G, U30G, and U40G accordingly (Scheme 5).



Scheme 5. Mixed (urea/glycerine) fuel SCS of γ -alumina, with varying number of moles of glycine (Ψ) [27].

X-ray diffraction (XRD) analysis of the synthesized γ -alumina powders revealed interesting phase changes. For instance, with the gradient increase of the glycine content in the fuel, there is a corresponding phase transition from pure α -alumina to a mixture of α - and γ -alumina (Figure 5) [27]. This shift in phases, from the high-temperature alpha phase to the low-temperature gamma phase is consistent even at theoretically high temperatures and enthalpy, and was attributed to incomplete combustion resulting from the high carbon content in glycine [90]. Furthermore, the TEM micrographs displayed the largest aggregate of crystallites with dimensions of 300 nm and crystallite size of 81 nm (Figure 6) at $\Psi = 0$ (corresponding to stoichiometric conditions). This is due to sintering of fine particles at elevated local temperatures [57,72]. However, the crystallite size decreases with the gradient additions of glycine into the fuel composition (i.e. $\Psi = 0.4, 0.8, 1.2, 1.6$) [27], which lowers the prevailing reaction temperature and consequently prevents particle sintering. The mixed fuel approach offers a custom-tailored γ -alumina structure with optimized morphology, uniformity, and specific surface characteristics, making it ideally suited for catalytic applications where these properties play a crucial role in achieving high catalytic activity and selectivity [91–93].

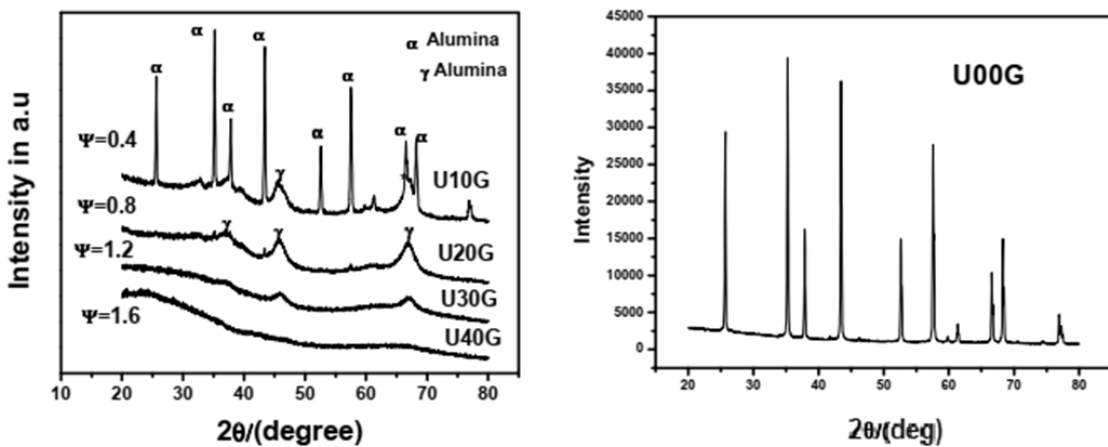


Figure 5. XRD patterns of the synthesized alumina samples showing phase transition from pure alpha alumina to a mixture of alpha and gamma alumina with a corresponding gradient increase of the glycine content in the mixed fuel composition. Reprinted with permission [27].

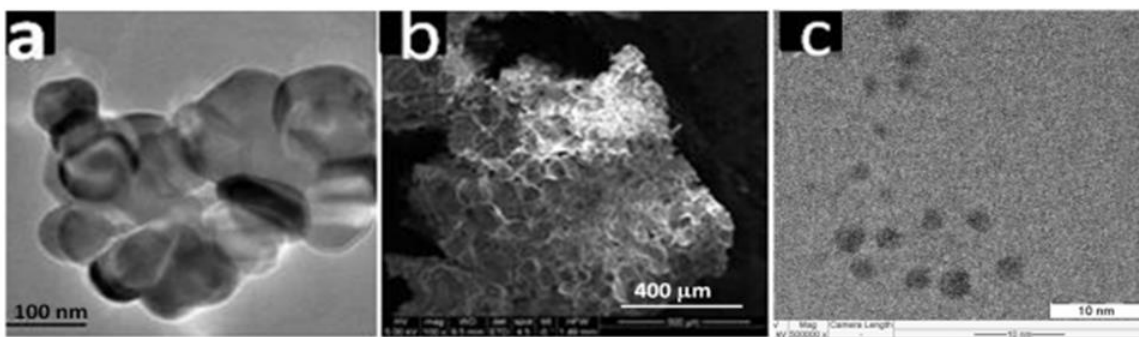


Figure 6. TEM images of synthesized alumina samples: (a) U00G, (b) U00G, and (c) U20G. Reprinted with permission [27].

4. Effect of Mixed Fuels on Combustion of Precursors, Physicochemical and Morphological Properties of the Synthesized Materials

This section discusses the effect of mixed fuels on the combustion reaction of precursors in SCS, and how the approach influences different physical and chemical properties, such as particle size, surface area, thermal decomposition temperature and rate, morphology and phase formation in the synthesized materials.

4.1. Adiabatic Flame Temperature of Combustion Reaction

As discussed earlier in this review, the three prevailing thermodynamic processes that occur during combustion synthesis are heat generation due to the exothermic reaction, gas evolution and powder crystallization. The overall effect of these afore-mentioned processes is on the size of the resulting powders. For instance, high combustion temperatures can result in the formation of relatively large crystallites due to crystal growth, while in some instances low temperature can prevent particle agglomeration and sintering [46,91]. This analogy is based on the ability of the fuel to increases the combustion temperature and enhance the sample crystallinity [35].

The studies on mixed fuel combustion synthesis of diverse materials for different applications have demonstrated the effect of mixing fuels on reaction parameters such as adiabatic flame temperatures, maximum temperature reached and the type of flame formed [27,94,95]. Sherikar and Umarji [27] prepared nano crystalline γ -alumina powders using a mixture of urea and glycine fuel as reducers. The result for theoretically calculated variation in adiabatic flame temperature as correlated with the measured flame temperatures demonstrated a direct proportionate relationship between the theoretical adiabatic temperature and the gradient addition of glycine to a maximum of 2020 K (at $\Psi = 1.6$). In contrast, an inverse relation is observed with the measured flame temperature.[27] The difference in temperature is thus attributed to more moles of gases formed during combustion, which consequently lead to reduced exothermicity of the reaction and incomplete combustion. Similarly, Gotoh et al. demonstrated that different phases of persistent phosphor $\text{Gd}_3\text{Al}_2\text{Ga}_3\text{O}_{12}:\text{Ce}^{3+}-\text{Cr}^{3+}$ (GAGG:Ce³⁺-Cr³⁺) material are formed when single glycine fuel or mixed fuels of glycine and urea at 773 K are used in a solution combustion synthesis [28]. In those reactions' conditions, a pure phase of GAGG: Ce³⁺-Cr³⁺ is obtained with the mixed glycine and urea fuel, while the use of either single fuel (glycine or urea) lead to incomplete combustion and amorphous products.

Sharma et al. also prepared alumina powders using similar nitrate metal precursor and mixed urea-glycine fuel SCS approach [96]. Their study highlighted a continuous change in the various characterisations of the powders with corresponding change in percentage combination of the two fuels. When the percentage of urea was higher than glycine, the reaction took place with high exothermicity and gave high crystallinity to the product phase, while amorphous character was observed in the cases when higher amounts of glycine were used. The high rate of combustion of urea fuel promotes agglomeration of particles, while the low combustion of glycine fuel promotes the formation of a small range of particles sizes [27]. Several other authors reported on the effect of exothermicity in the SCS reaction when the glycine was used in a fuel mixture [41,46,90]. In all these studies, the ability of glycine to provide lower rate of combustion was clearly demonstrated. Such systems are prone to incomplete combustion or combustion with residual carbon content in product phase. In contrast, systems that are based on increasing urea in mix fuel approach increases the extent of exothermicity in solution combustion [96].

In relation to the effect of mixed fuel on the adiabatic condition for solution combustion synthesis, Khaliullin et al. compiled a list of the temperature effect due the urea/glycine mixture as presented in Table 3 [97]. It follows that some nitrate metal precursors cannot undergo redox reaction with any fuel. For instance, a mixture of calcium nitrate with urea might not be ignited altogether, while an explosive reaction could be established with β -alanine [98].

Table 3. Temperature effect ΔT_{ad} for adiabatic SCS reactions involving glycine and urea as adopted from Khaliullin et al. [97].

Product	ΔT_{ad} K (glyc/urea)	Product	ΔT_{ad} , K (glyc/urea)	Product	ΔT_{ad} K (glyc/urea)
Li ₂ O	2148/1763	LiOH	2511/2106	Li ₂ CO ₃	2885/2436
Na ₂ O	1502/1199	NaOH	2063/1722	Na ₂ CO ₃	2596/2169
K ₂ O	1123/857	KOH	1830/1519	K ₂ CO ₃	2435/2051
Rb ₂ O	1019/762	RbOH	1703/1410	Rb ₂ CO ₃	2321/1952
Cs ₂ O	885/643	CsOH	1673/1381	Cs ₂ CO ₃	2255/1898
BeO	3910/3292	Be(OH) ₂	4043/3422	BeCO ₃	3969/3349
MgO	2977/2484	Mg(OH) ₂	3219/2710	MgCO ₃	3358/2825
CaO	2488/2053	Ca(OH) ₂	2779/2331	CaCO ₃	3121/2627
SrO	2165/1766	Sr(OH) ₂	2636/2182	SrCO ₃	3052/2561
BaO	1954/1561	Ba(OH) ₂	2401/2004	BaCO ₃	2928/2456
Al ₂ O ₃	3048/2526	Al(OH) ₃	3273/2731	Al ₂ (CO ₃) ₃	3377/2819
Ga ₂ O ₃	3632/3055	Ga(OH) ₃	3897/3292	Ga ₂ (CO ₃) ₃	3849/3249
In ₂ O ₃	3364/2816	In(OH) ₃	3603/3029	In ₂ (CO ₃) ₃	3533/2967
Sc ₂ O ₃	3083/2563	Sc(OH) ₃	3238/2702	Sc ₂ (CO ₃) ₃	3308/2763
Y ₂ O ₃	2740/2265	Y(OH) ₃	3041/2534	Y ₂ (CO ₃) ₃	3241/2713
La ₂ O ₃	2804/2326	La(OH) ₃	3162/2651	La ₂ (CO ₃) ₃	3405/2863
TiO ₂	3043/2571	Ti(OH) ₄	1696/1358	Ti(CO ₃) ₂	2155/1703
ZrO ₂	2636/2205	Zr(OH) ₄	1372/1059	Zr(CO ₃) ₂	1821/1415
HfO ₂	2546/2130	Hf(OH) ₄	1173/891	Hf(CO ₃) ₂	1629/1252
MnO	2679/2226	Mn(OH) ₂	2963/2481	MnCO ₃	3110/2614
FeO	2690/2245	Fe(OH) ₂	2942/2467	FeCO ₃	3069/2578
CoO	2816/2367	Co(OH) ₂	3036/2565	CoCO ₃	3106/2628
NiO	2955/2474	Ni(OH) ₂	3135/2636	NiCO ₃	3315/2797
Fe ₂ O ₃	3084/2574	Fe(OH) ₃	3215/2694	Fe ₂ (CO ₃) ₃	3236/2709

4.2. Thermal Decomposition Rate and Temperature

Fuels such as CTAB have higher decomposition temperatures and slower combustion rates than glycine and citric acid [99]. However, the combination of CTAB with other fuels such as citric acid and glycine can decrease the decomposition temperature while increasing the combustion reaction rate [13]. The fast combustion reaction rate observed when glycine is used as a second fuel is ascribed to the exothermic reaction of hypergolic gases such as NO_x, NH₃, CO, etc. formed during the decomposition of the metal nitrate and the fuel [16].

In a related work by Hamedani et al.; the use of glycine as a mixed fuel with CTAB to synthesize CoFe₂O₄ powders gave higher combustibility due to its lower decomposition temperature as compared to that of CTAB fuel [45]. The mixed fuel showed higher weight loss and exothermic temperature than those of single fuels, indicating a slower decomposition rate. Other studies corroborated the afore mentioned and revealed that rates of combustion reaction are higher in the samples via mixed urea and glycine fuel when compared to those from the respective single fuels [35].

4.3. Particle Size

Some fuel systems in combustion synthesis serve as structure-directing templates and give tuneable surface properties in metal oxide nanomaterials for potential applications in catalysis, optoelectronics, and gas sensors [30,100,101]. The use of the mixed fuel combustion synthesis facilitates the reduction in particle size, when compared to the analogous product formed using a single fuel. This is achieved through control of flame temperature and the type and amount of released gaseous products [26,46]. Asefi et al. noted that BiFeO_3 powders prepared from a mixture glycine and urea had lower crystallite sizes when compared to the powders prepared using the single fuels [31]. This is been made in similar reported studies, and is attributed to the lowering of the combustion temperature, the evolution of a large volumes of gas (CO_2 and H_2O) and a less violent reaction caused by the addition of glycine [27,31,46,72,96].

It was observed in a study on the preparation of hierarchical porous LiFePO_4 powders for lithium-ion batteries by Karami et al. [54] that a combination with a fuel such as glycine, with a high heat content is expected to increase the combustion rate. Morphological analysis of the LiFePO_4 as-synthesized powders obtained showed that the crystallite size increased with the content of CTAB in the fuel, while the opposite is observed for the mixed CTAB-glycine. On the other hand, Lazarova et al. used a mixture of glycine-glycerol to prepare nano-sized spinel manganese ferrites [MnFe_2O_4] at different reducing power ratios [102]. Thus far, this is the only reported study whose findings oppose the generalized pattern, especially when glycine is used in a mixed fuel combustion synthesis. The report showed that the synthesized sample from the highest amount of glycine in the fuel has five times larger crystallite sizes than synthesized samples obtained from other fuel mixtures (Figure 7). Their argument is the only outlier in the literature that suggests glycine decreases the exothermicity of a reaction thereby preventing agglomeration and sintering of the synthesized material [46,91].

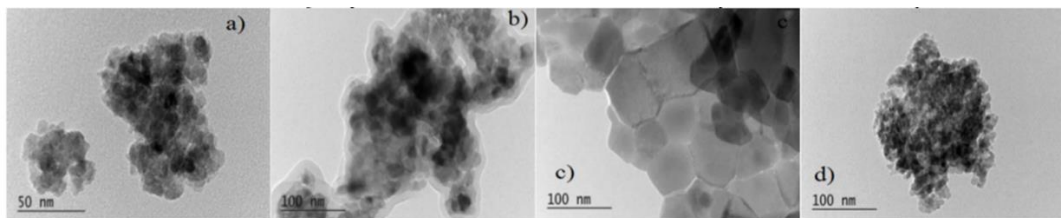


Figure 7. TEM images of synthesized nano-sized MnFe_2O_4 using a mixture of fuels: (a) sucrose-urea (3:1), (b) sucrose-urea (1:3), both at 500 °C; and (c) glycine-glycerol (3:1) at 400 and (d) glycine-glycerol (1:3) at 500 °C under inert conditions. Reprinted with permission [102].

4.4. Surface Area

It is generally accepted that the liberation of a large amount of gaseous products such H_2O , CO_2 , N_2 , H_2 , and CO during the combustion reaction leads to the formation of a spongy and porous structure [21,25,103]. A recent study has showed that mixed fuels made up of urea and glycine for the synthesis of Fe_3O_4 powders produced foamy and sponge-like material, due to the release of large amount of gases, within shorter combustion time [39]. These characteristic favours the synthesis of porous powders and inhibits particle agglomeration [28,39,54]. However, work by Meza-Trujillo et al.[104,105] refuted the generally acceptable norm as their use of a mixture of urea and β -alanine could not produce a porous material, likely due to the high temperature attained during the combustion reaction which prompted sintering of the grains. The textural properties were only improved by the addition of oxalic acid which acted as a heterogeneous and combustion retarding agent [105].

The use of activated carbon as a secondary fuel at different fuel-oxidant ratios in the combustion synthesis of ZnO produced porous material with excellent morphological property for photocatalytic dye removal [106]. Morphological analysis of the synthesized ZnO revealed that the presence of the secondary fuel had a profound effect on reducing crystallite size and enhancement of specific surface area. The crystallite size of the synthesized ZnO powders varied from 46 to 26 nm, with the powder prepared at a fuel-oxidant ratio of 1.8, which gave possessing the lowest crystallite size and high

specific surface area of $69 \text{ m}^2/\text{g}$ [106]. The excellent absorption and photocatalytic ability of the powder when applied as dye remover is attributed to the synergistic interaction and interplay of enhanced surface area and catalytic ability of the material [101].

4.5. Material Phases

Alumina powders via combustion synthesis of glycine and urea mixed fuels exist in both the amorphous and crystalline material phases depending on the ratio of the fuel mixture [96]. Powders prepared with a higher content of urea displayed increased crystallinity, while samples with a higher content of glycine are generally amorphous. These observations reveal that the ratio of the constituent fuels influences phase changes in the material product. In the case of the alumina powders, urea promotes crystallinity, and glycine promotes amorphous character in the product phase. The formation of amorphous phases is attributed to the lack of sufficient temperature to promote alumina crystallisation [96]. Similarly, an increase in the glycine content led to a phase change to amorphous in the case of the mixed (urea and glycine) fuel combustion synthesis of alumina [27]. The change in phases from the high temperature α -corundum phase to the low temperature γ -phase and amorphous phase was reported to be due to incomplete combustion taking place as a result of high number of carbon atoms present in glycine [27,94].

Studies on single and mixed fuel combustion syntheses of FeCr_2O_4 powders for application in pigments revealed that phase changes are also influenced by the constituent mixed fuels used [29,107,108]. In this vein, the use of mixed citric acid and ethylene glycol fuels yield amorphous phases, while the synthesized powders prepared using the glycine fuel resulted in narrower and higher peak intensities in the XRD patterns of the products due to stronger combustion than the urea [107,108]. Subsequent addition of glycine to urea, citric acid, or ethylene glycol ensured higher reactivity in all the corresponding fuel mixtures, and results in the formation of corresponding highly crystalline FeCr_2O_4 samples. The arrangement of common organic fuels in order of reactivity follows glycine > urea > citric acid > ethylene glycol. Based on this, it is deducible that the mixed fuel constituents and the fuel mixing ratio affect surface phases as evident from the associated XRD patterns and FTIR spectra of the synthesized samples [29]. The synthesis of powders with glycine-containing fuel mixture led to the strongest combustion reaction resulting in the highest crystallinity and the lowest lattice parameters.

5. Summary, Conclusion and Future Directions

This paper reviewed the uniqueness of the mixed fuel approach in the Solution Combustion Synthesis of nanomaterials for various applications. The consideration of the triplex function of the fuel, and innovative advantages of SCS over its contemporaries led to the growing interest in mixed fuel combustion synthesis.

Diverse applications of the nanomaterials obtained from mixed fuel SCS in catalysis, dielectric, recycling and recoveries of spent LiBs, energy cells, and optics, are highlighted in this review. Whereas the corresponding effect of the mixed fuel system on the combustion and decomposition rates of the precursors as well as on the materials' physicochemical and morphological properties are discussed in earnest. The synthetic routes and data from the various characterization techniques like TEM and XRD, are used in analyzing and comparing these properties with those reported for analogous as-synthesized materials from single fuel SCS.

The characteristics of fuels used in SCS such as molecular structure, functional groups, decomposition temperature, etc., influence their prevailed combustion features such as combustion reaction rate, combustion temperature, etc. The use of glycine as a fuel in combustion synthesis is promoted by its high combustion rate and temperature, low chelating ability and, hence, results in the low agglomeration and smaller crystallite sizes in the corresponding as-synthesized materials. High molecular weight fuels such as CTAB have slow combustion rates and, hence, mixing with glycine, for instance, increases the combustion rate. Polyfunctional fuels in mixtures have greater tendency to increase the amount of gases evolved during combustion. Thus, the higher

decomposition temperature and a slow decomposition rate in CTAB made it comparatively unsuitable for combination with citric acid, which is characterized as having high adiabatic temperature due to low rate of decomposition. In relation to this, common organic fuels follow the order of reactivity viz; glycine > urea > citric acid > ethylene glycol. The synthesis of powders using glycine as fuel led to the strongest reaction resulting in the highest crystallinity and the lowest lattice parameters. It is then deducible that the nature of the mixed fuel constituents and the fuel mixing ratio affect XRD patterns, FTIR spectra and other characterization spectra of the resultant samples. Hence, with the current emphasis on more environmentally sustainable and benign synthetic routes to chemicals and materials for diverse applications, the prospects are infinite for the usage of mixed fuel SCS.

Author Contributions: Conceptualization, S.P., H.I. and P.N.; methodology, S.P., H.I. and P.N.; software, H.I.; validation, S.P., H.I., H.B.F., E.J.O. and P.N.; formal analysis, S.P., H.I., H.B.F., E.J.O. and P.N.; investigation, S.P., H.I., H.B.F., E.J.O. and P.N.; resources, H.I. and P.N.; data curation, S.P., H.I. and P.N.; writing—original draft preparation, S.P., H.I. and P.N.; writing—review and editing, S.P., H.I., H.B.F., E.J.O. and P.N.; visualization, H.I., H.B.F., E.J.O. and P.N.; supervision, P.N., H.B.F. and E.J.O.; project administration, P.N.; funding acquisition, P.N. All authors have read and agreed to the published version of the manuscript.

Funding: This research was supported by DUT and DHET.

Data Availability Statement: The data sets generated during and/or analyzed during the current study are available from the corresponding author on reasonable request.

Acknowledgments: DUT/HANT is acknowledged for funding the postdoctoral fellowship of H.I.

Conflicts of Interest: The authors declare no conflict of interest. The funding sponsors had no role in the design of the study; in the collection, analyses, or interpretation of data; in the writing of the manuscript, and in the decision to publish the results.

Abbreviations

The following abbreviations are used in this manuscript:

Cit	Citric acid
CS	Combustion Synthesis
CTAB	Cetyltrimethylammonium bromide
EDX	Energy Dispersive X-ray
En	Ethylenediamine
En/Cit	Ethylenediamine/Citric acid
En/Ox	Ethylenediamine/Oxalic acid
En/Ox/Cit	Ethylenediamine, Oxalic acid, and Citric acid
FESEM	Field-Emission Scanning Electron Microscopy
FTIR	Fourier Transform Infrared
LIBs	Lithium-ion Batteries
LSM	Lanthanum Strontium Manganite
Ox/Cit	Oxalic acid/Citric acid
Ox	Oxalic acid
PVP	polyvinylpyrrolidone
SAED	Selected Area Electron Diffraction
SCS	Solution Combustion Synthesis
SOFC	Solid Oxide Fuel Cell
STA	Simultaneous Thermal Analysis
TEM	Transmission Electron Microscopy
UV	Ultraviolet
XRD	X-ray Diffraction

References

1. Anastas, P.T. Introduction: Green Chemistry. *Chem Rev.* **2007**, *107*, 2167-2168. <https://doi.org/10.1021/cr0783784>.
2. Kingsley, J.; Patil, K. A novel combustion process for the synthesis of fine particle α -alumina and related oxide materials. *Mater Lett.* **1988**, *6*, 427-432. [https://doi.org/10.1016/0167-577X\(88\)90045-6](https://doi.org/10.1016/0167-577X(88)90045-6)
3. Novitskaya, E.; Kelly, J.P.; Bhaduri, S.; Graeve, O.A. A review of solution combustion synthesis: an analysis of parameters controlling powder characteristics. *Int Mater Rev.* **2021**, *66*, 188-214. <https://doi.org/10.1080/09506608.2020.1765603>
4. Mirbagheri, S.; Masoudpanah, S.; Alamolhoda, S. Structural and optical properties of $ZnAl_2O_4$ powders synthesized by solution combustion method: Effects of mixture of fuels. *Optik.* **2020**, *204*, 164170-164177. <https://doi.org/10.1016/j.ijleo.2020.164170>
5. Deganello, F.; Liotta, L.F.; Marcì, G.; Fabbri, E.; Traversa, E. Strontium and iron-doped barium cobaltite prepared by solution combustion synthesis: exploring a mixed-fuel approach for tailored intermediate temperature solid oxide fuel cell cathode materials. *Mater Renew Sustain Energy.* **2013**, *2*, 1-14. <https://doi.org/10.1007/s40243-013-0008-z>
6. Deganello, F.; Tyagi, A.K. Solution combustion synthesis, energy and environment: Best parameters for better materials. *Prog Cryst Growth Charact Mater.* **2018**, *64*, 23-61. <https://doi.org/10.1016/j.pcrysgrow.2018.03.001>
7. Gao, R.; Sun, C.; Zhou, T.; Zhuang, L.; Xie, H. Recycling of $LiNi_{0.5}Co_{0.2}Mn_{0.3}O_2$ Material from Spent Lithium-ion Batteries Using Mixed Organic Acid Leaching and Sol-gel Method. *ChemistrySelect.* **2020**, *5*, 6482-6490. <https://doi.org/10.1002/slct.202001843>
8. Siddique, F.; Gonzalez-Cortes, S.; Mirzaei, A.; Xiao, T.; Rafiq, M.; Zhang, X. Solution combustion synthesis: the relevant metrics for producing advanced and nanostructured photocatalysts. *Nanoscale.* **2022**, *14*, 11806-11868. <https://doi.org/10.1039/d2nr02714c>
9. Ghadimi Mahanipour, H.; Masoudpanah, S.M.; Adeli, M.; Hoseini, S.M.H. Regeneration of $LiNi_{0.6}Co_{0.2}Mn_{0.2}O_2$ material from spent lithium-ion batteries by solution combustion synthesis method. *J Energy Storage.* **2024**, *79*, 110192-110201. <https://doi.org/10.1016/j.est.2023.110192>.
10. Masokano, D.S.; Ntola, P.; Mahomed, A.S.; Bala, M.D.; Friedrich, H.B. Influence of support properties on the activity of $2Cr-Fe/MgO-MO_2$ catalysts ($M= Ce, Zr, CeZr$ and Si) for the dehydrogenation of n-octane with CO_2 . *J CO_2 Util.* **2024**, *86*, 102909-102922. <https://doi.org/10.1016/j.jcou.2024.102909>
11. Ntola, P.; Friedrich, H.B.; Singh, S.; Olivier, E.J.; Farahani, M.; Mahomed, A.S. Effect of the fuel on the surface VO_x concentration, speciation and physico-chemical characteristics of solution combustion synthesised VO_x/MgO catalysts for n-octane activation. *Catal Comm.* **2023**, *174*, 106571. <https://doi.org/10.1016/j.catcom.2022.106571>.
12. Chupakhina, T.I.; Melnikova, N.V.; Kadyrova, N.I.; Mirzorakhimov, A.; Tebenkov, A.V.; Deeva, Y.A.; Zainulin, Y.G.; Gyrdasova, O.I. Synthesis, structure and dielectric properties of new ceramics with K_2NiF_4 -type structure. *J Eur Ceram Soc.* **2019**, *39*, 3722-3729. <https://doi.org/10.1016/j.jeurceramsoc.2019.05.018>
13. Masoudpanah, S.; Alamolhoda, S. Solution combustion synthesis of $LiMn_{1.5}Ni_{0.5}O_4$ powders by a mixture of fuels. *Ceram Int.* **2019**, *45*, 22849-22853. <https://doi.org/10.1016/j.ceramint.2019.07.327>
14. Xu, S.-L.; Zhao, S.; Zeng, W.-J.; Li, S.; Zuo, M.; Lin, Y.; Chu, S.; Chen, P.; Liu, J.; Liang, H.-W. Synthesis of a Hexagonal-Phase Platinum-Lanthanide Alloy as a Durable Fuel-Cell-Cathode Catalyst. *Chem Mater.* **2022**, *34*, 10789-10797. <https://doi.org/10.1021/acs.chemmater.2c03219>
15. Zareba, J.K.; Nyk, M.; Samoć, M. Nonlinear Optical Properties of Emerging Nano-and Microcrystalline Materials. *Adv Opt Mater.* **2021**, *9*, 2100216-2100250. <https://doi.org/10.1002/adom.202100216>
16. Vasei, H.V.; Masoudpanah, S.; Adeli, M.; Aboutalebi, M. Photocatalytic properties of solution combustion synthesized ZnO powders using mixture of CTAB and glycine and citric acid fuels. *Adv Powder Technol.* **2019**, *30*, 284-291. <https://doi.org/10.1016/j.apt.2018.11.004>
17. Ahmad, I.; Akhtar, M.S.; Ahmed, E.; Ahmad, M.; Keller, V.; Khan, W.Q.; Khalid, N. Rare earth co-doped ZnO photocatalysts: Solution combustion synthesis and environmental applications. *Sep Purif Technol.* **2020**, *237*, 116328-116340. <https://doi.org/10.1016/j.seppur.2019.116328>

18. Carlos, E.; Martins, R.; Fortunato, E.; Branquinho, R. Solution Combustion Synthesis: Towards a Sustainable Approach for Metal Oxides. *Chem Eur J.* **2020**, *26*, 9099-9125. <https://doi.org/10.1002/chem.202000678>
19. Cao, Z.; Zuo, C. In situ synthesis of chromium carbide nanocomposites from solution combustion synthesis precursors. *J Mol Struct.* **2019**, *1175*, 496-503. <https://doi.org/10.1016/j.molstruc.2018.08.008>
20. Roslyakov, S.; Yermekova, Z.; Trusov, G.; Khort, A.; Evdokimenko, N.; Bindug, D.; Karpenkov, D.; Zhukovskyi, M.; Degtyarenko, A.; Mukasyan, A. One-step solution combustion synthesis of nanostructured transition metal antiperovskite nitride and alloy. *Nano-Struct Nano-Objects.* **2021**, *28*, 100796-100809. <https://doi.org/10.1016/j.nanoso.2021.100796>
21. Mukasyan, A.S. Combustion synthesis of boron nitride ceramics: fundamentals and applications. *Nitride Ceramics: Combustion Synthesis, Properties, and Applications.* **2014**, 49-74. <https://doi.org/10.1002/9783527684533.ch2>
22. Ramesh, A.; Gavaskar, D.; Nagaraju, P.; Duvvuri, S.; Vanjari, S.R.K.; Subrahmanyam, C. Mn-doped ZnO microspheres prepared by solution combustion synthesis for room temperature NH₃ sensing. *Appl Surf Sci Adv.* **2022**, *12*, 100349-100360. <https://doi.org/10.1016/j.apsadv.2022.100349>
23. Ntola, P.; Friedrich, H.B.; Mahomed, A.S.; Olivier, E.J.; Govender, A.; Singh, S. Exploring the role of fuel on the microstructure of VO_x/MgO powders prepared using solution combustion synthesis. *Mater Chem Phys.* **2022**, *278*, 125602-125613. <https://doi.org/10.1016/j.matchemphys.2021.125602>
24. Chandradass, J.; Balasubramanian, M.; Kim, K.H. Synthesis and characterization of LaAlO₃ nanopowders by various fuels. *Mater Manuf Process.* **2010**, *25*, 1449-1453. <https://doi.org/10.1080/10426914.2010.508962>
25. Varma, A.; Mukasyan, A.S.; Rogachev, A.S.; Manukyan, K.V. Solution combustion synthesis of nanoscale materials. *Chem Rev.* **2016**, *116*, 14493-14586. <https://doi.org/10.1021/acs.chemrev.6b00279>
26. Tarragó, D.P.; Malfatti, C.d.F.; de Sousa, V.C. Influence of fuel on morphology of LSM powders obtained by solution combustion synthesis. *Powder Technol.* **2015**, *269*, 481-487. <https://doi.org/10.1016/j.powtec.2014.09.037>
27. Sherikar, B.N.; Umarji, A.M. Synthesis of γ -alumina by solution combustion method using mixed fuel approach (urea+ glycine fuel). *Int J Res Eng Technol.* **2013**, *5*, 434-438. <https://doi.org/10.15623/IJRET.2013.0213082>
28. Gotoh, T.; Jeem, M.; Zhang, L.; Okinaka, N.; Watanabe, S. Synthesis of yellow persistent phosphor garnet by mixed fuel solution combustion synthesis and its characteristic. *J Phys Chem Solids.* **2020**, *142*, 109436-109443. <https://doi.org/10.1016/j.jpcs.2020.109436>
29. Paborji, F.; Shafiee Afarani, M.; Arabi, A.M.; Ghahari, M. Solution combustion synthesis of FeCr₂O₄ powders for pigment applications: Effect of fuel type. *Int J Appl Ceram Technol.* **2022**, *19*, 2406-2418. <https://doi.org/10.1111/ijac.14071>
30. Shukla, R.; Tyagi, A. Combustion synthesis: a versatile method for functional materials, Handbook on synthesis strategies for advanced materials: volume-I: techniques and fundamentals. **2021**, 51-78. https://doi.org/10.1007/978-981-16-1807-9_2
31. Asefi, N.; Masoudpanah, S.; Hasheminiasari, M. Photocatalytic performances of BiFeO₃ powders synthesized by solution combustion method: The role of mixed fuels. *Mater Chem Phys.* **2019**, *228*, 168-174. <https://doi.org/10.1016/j.matchemphys.2019.02.059>
32. Thoda, O.; Xanthopoulou, G.; Vekinis, G.; Chroneos, A. Review of recent studies on solution combustion synthesis of nanostructured catalysts. *Adv Eng Mater.* **2018**, *20*, 1800047-1800077. <https://doi.org/10.1002/adem.201800047>
33. Khaliullin, S.M.; Koshkina, A. Influence of fuel on phase formation, morphology, electric and dielectric properties of iron oxides obtained by SCS method. *Ceram Int.* **2021**, *47*, 11942-11950. <https://doi.org/10.1016/j.ceramint.2021.01.035>
34. Ianoş, R.; Lazău, I.; Păcurariu, C.; Barvinschi, P. Fuel mixture approach for solution combustion synthesis of Ca₃Al₂O₆ powders. *Cem Concr Res.* **2009**, *39*, 566-572. <https://doi.org/10.1016/j.cemconres.2009.03.014>
35. Ianoş, R.; Istratie, R.; Păcurariu, C.; Lazău, R. Solution combustion synthesis of strontium aluminate, SrAl₂O₄, powders: single-fuel versus fuel-mixture approach. *Phys Chem Chem Phys.* **2016**, *18*, 1150-1157. <https://doi.org/10.1039/C5CP06240C>

36. Bai, J.; Liu, J.; Li, C.; Li, G.; Du, Q. Mixture of fuels approach for solution combustion synthesis of nanoscale MgAl₂O₄ powders. *Adv Powder Technol.* **2011**, *22*, 72-76. <https://doi.org/10.1016/j.apt.2010.03.013>

37. Chandradass, J.; Kim, K.H. Mixture of fuels approach for the solution combustion synthesis of LaAlO₃ nanopowders. *Adv Powder Technol.* **2010**, *21*, 100-105. <https://doi.org/10.1016/j.apt.2009.10.014>

38. Aruna, S.; Rajam, K. Mixture of fuels approach for the solution combustion synthesis of Al₂O₃-ZrO₂ nanocomposite. *Mater Res Bull.* **2004**, *39*, 157-167. <https://doi.org/10.1016/j.materresbull.2003.10.005>

39. Parnianfar, H.; Masoudpanah, S.; Alamolhoda, S.; Fathi, H. Mixture of fuels for solution combustion synthesis of porous Fe₃O₄ powders. *J Magn Magn Mater.* **2017**, *432*, 24-29. <https://doi.org/10.1016/j.jmmm.2017.01.084>

40. Hadadian, S.; Masoudpanah, S.; Alamolhoda, S. Solution combustion synthesis of Fe₃O₄ powders using mixture of CTAB and citric acid fuels. *J Supercond Nov Magn.* **2019**, *32*, 353-360. <https://doi.org/10.1007/s10948-018-4685-9>

41. Kalantari Bolaghi, Z.; Hasheminiasari, M.; Masoudpanah, S.M. Solution combustion synthesis of ZnO powders using mixture of fuels in closed system. *Ceram Int.* **2018**, *44*, 12684-12690. <https://doi.org/10.1016/j.ceramint.2018.04.069>

42. Aruna, S.; Kini, N.; Rajam, K. Solution combustion synthesis of CeO₂-CeAlO₃ nano-composites by mixture-of-fuels approach. *Mater Res Bull.* **2009**, *44*, 728-733. <https://doi.org/10.1016/j.materresbull.2008.09.034>

43. Sasikumar, S.; Vijayaraghavan, R. Solution combustion synthesis of bioceramic calcium phosphates by single and mixed fuels—a comparative study. *Ceram Int.* **2008**, *34*, 1373-1379. <https://doi.org/10.1016/j.ceramint.2007.03.009>

44. Aali, H.; Azizi, N.; Baygi, N.J.; Kermani, F.; Mashreghi, M.; Youssefi, A.; Mollazadeh, S.; Khaki, J.V.; Nasiri, H. High antibacterial and photocatalytic activity of solution combustion synthesized Ni_{0.5}Zn_{0.5}Fe₂O₄ nanoparticles: Effect of fuel to oxidizer ratio and complex fuels. *Ceram Int.* **2019**, *45*, 19127-19140. <https://doi.org/10.1016/j.ceramint.2019.06.159>

45. Famenin Nezhad Hamedani, S.; Masoudpanah, S.; Bafghi, M.S.; Asgharinezhad Baloochi, N. Solution combustion synthesis of CoFe₂O₄ powders using mixture of CTAB and glycine fuels. *J Sol-Gel Sci Technol.* **2018**, *86*, 743-750. <https://doi.org/10.1007/s10971-018-4671-5>

46. Naveenkumar, A.; Kuruva, P.; Shivakumara, C.; Srilakshmi, C. Mixture of Fuels Approach for the Synthesis of SrFeO₃- δ Nanocatalyst and Its Impact on the Catalytic Reduction of Nitrobenzene. *Inorg Chem.* **2014**, *53*, 12178-12185. <https://doi.org/10.1021/ic502121k>

47. Vasei, H.V.; Masoudpanah, S.M.; Adeli, M.; Aboutalebi, M.R. Solution combustion synthesis of ZnO powders using CTAB as fuel. *Ceram Int.* **2018**, *44*, 7741-7745. <https://doi.org/10.1016/j.ceramint.2018.01.202>

48. Lin, J.; Wen, Z.; Xu, X.; Li, N.; Song, S. Characterization and improvement of water compatibility of γ -LiAlO₂ ceramic breeders. *Fusion Eng Des.* **2010**, *85*, 1162-1166. <https://doi.org/10.1016/j.fusengdes.2010.02.027>

49. Wen, Z.; Gu, Z.; Xu, X.; Zhu, X. Research on the preparation, electrical and mechanical properties of γ -LiAlO₂ ceramics. *J Nucl Mater.* **2004**, *329*, 1283-1286. <https://doi.org/10.1016/j.jnucmat.2004.04.230>

50. Zhuravlev, V.D.; Reznitskikh, O.G.; Ermakova, L.V.; Patrusheva, T.A.; Nefedova, K.V. Simultaneous Thermal Analysis of Lithium Aluminate SCS-Precursors Produced with Different Fuels. *Int J Self-Propagating High-Temp Synth.* **2023**, *32*, 208-214. <https://doi.org/10.3103/S1061386223030111>

51. Sharifidarabad, H.; Zakeri, A.; Adeli, M. Preparation of spinel LiMn₂O₄ cathode material from used zinc-carbon and lithium-ion batteries. *Ceram Int.* **2022**, *48*, 6663-6671. <https://doi.org/10.1016/j.ceramint.2021.11.216>

52. Adams, R.A.; Pol, V.G.; Varma, A. Tailored solution combustion synthesis of high performance ZnCo₂O₄ anode materials for lithium-ion batteries. *Ind Eng Chem Res.* **2017**, *56*, 7173-7183. <https://doi.org/10.1021/acs.iecr.7b00295>

53. Chen, M.; Zhang, Y.; Xing, G.; Chou, S-L.; Tang, Y. Electrochemical energy storage devices working in extreme conditions. *Energy Environ Sci.* **2021**, *14*, 3323-3351. <https://doi.org/10.1039/D1EE00271F>

54. Karami, M.; Masoudpanah, S.; Rezaie, H. Solution combustion synthesis of hierarchical porous LiFePO₄ powders as cathode materials for lithium-ion batteries. *Adv Powder Technol.* **2021**, *32*, 1935-1942. <https://doi.org/10.1016/j.apt.2021.04.007>

55. Karami, M.; Masoudpanah, S.M.; Rezaei, H.R. Electrochemical Performance of LiFePO₄/C Powders Synthesized by Solution Combustion Method as the Lithium-Ion Batteries Cathode Material. *J Adv Mater Technol.* **2022**, *11*, 81-93. <https://doi.org/10.30501/jamt.2022.297161.1186>

56. Xu, H.; Zhao, Y.; Wang, Q.; He, G.; Chen, H. Supports promote single-atom catalysts toward advanced electrocatalysis. *Coord Chem Rev.* **2022**, *451*, 214261-214280. <https://doi.org/10.1016/j.ccr.2021.214261>

57. Wu, C.; Wang, Y.; Wu, K.; Zhai, H.; Gong, Z.; Peng, Z.; Jin, S.; Du, Q.; Jiao, K. Sintering kinetics and microstructure analysis of composite mixed ionic and electronic conducting electrodes. *Int J Energy Res.* **2022**, *46*, 8240-8255. <https://doi.org/10.1002/er.7726>

58. Ivanishchev, A.V.; Bobrikov, I.A.; Ivanishcheva, I.A.; Ivanshina, O.Y. Study of structural and electrochemical characteristics of LiNi_{0.33}Mn_{0.33}Co_{0.33}O₂ electrode at lithium content variation. *J Electroanal Chem.* **2018**, *821*, 140-151. <https://doi.org/10.1016/j.jelechem.2018.01.020>

59. Sommerville, R.; Zhu, P.; Rajaeifar, M.A.; Heidrich, O.; Goodship, V.; Kendrick, E. A qualitative assessment of lithium ion battery recycling processes. *Resour Conserv Recycl.* **2021**, *165*, 105219-105230. <https://doi.org/10.1016/j.resconrec.2020.105219>

60. Xing, L.; Lin, S.; Yu, J. Novel recycling approach to regenerate a LiNi_{0.6}Co_{0.2}Mn_{0.2}O₂ cathode material from spent lithium-ion batteries. *Ind Eng Chem Res.* **2021**, *60*, 10303-10311. <https://doi.org/10.1021/acs.iecr.1c01151>

61. Zheng, J.; Zhou, W.; Ma, Y.; Jin, H.; Guo, L. Combustion synthesis of LiNi_{1/3}Co_{1/3}Mn_{1/3}O₂ powders with enhanced electrochemical performance in LIBs. *J Alloys Compd.* **2015**, *635*, 207-212. <https://doi.org/10.1016/j.jallcom.2015.02.114>

62. Li, W.; Yao, L.; Zhang, X.; Lang, W.; Si, J.; Yang, J.; Li, L. The effect of chelating agent on synthesis and electrochemical properties of LiNi_{0.6}Co_{0.2}Mn_{0.2}O₂. *SN Appl Sci.* **2020**, *2*, 1-8. <https://doi.org/10.1007/s42452-020-2377-0>

63. Chamyani, S.; Salehirad, A.; Oroujzadeh, N.; Fateh, D.S. Effect of fuel type on structural and physicochemical properties of solution combustion synthesized CoCr₂O₄ ceramic pigment nanoparticles. *Ceram Int.* **2018**, *44*, 7754-7760. <https://doi.org/10.1016/j.ceramint.2018.01.205>

64. Jain, S.; Adiga, K.; Verneker, V.P. A new approach to thermochemical calculations of condensed fuel-oxidizer mixtures. *Combust Flame.* **1981**, *40*, 71-79. [https://doi.org/10.1016/0010-2180\(81\)90111-5](https://doi.org/10.1016/0010-2180(81)90111-5)

65. Balakrishnan, A.; Pizette, P.; Martin, C.; Joshi, S.; Saha, B. Effect of particle size in aggregated and agglomerated ceramic powders. *Acta Mater.* **2010**, *58*, 802-812. <https://doi.org/10.1016/j.actamat.2009.09.058>

66. Mestre, S.; Palacios, M.; Agut, P. Solution combustion synthesis of (Co, Fe) Cr₂O₄ pigments. *J Eur Ceram Soc.* **2012**, *32*, 1995-1999. <https://doi.org/10.1016/j.jeurceramsoc.2011.11.044>

67. Gilabert, J.; Palacios, M.D.; Sanz, V.; Mestre, S. Fuel effect on solution combustion synthesis of Co (Cr, Al) ₂O₄ pigments. *Bol Soc Esp Ceram Vidr.* **2017**, *56*, 215-225. <https://doi.org/10.1016/j.bsecv.2017.03.003>

68. Dwivedi, S. Solid oxide fuel cell: Materials for anode, cathode and electrolyte. *Int J Hydrogen Energy.* **2020**, *45*, 23988-24013. <https://doi.org/10.1016/j.ijhydene.2019.11.234>

69. Sun, C.; Hui, R.; Roller, J. Cathode materials for solid oxide fuel cells: a review. *J Solid State Electrochem.* **2010**, *14*, 1125-1144. <https://doi.org/10.1007/s10008-009-0932-0>

70. Yang, X-Y.; Chen, L-H.; Li, Y.; Rooke, J.C.; Sanchez, C.; Su, B-L. Hierarchically porous materials: synthesis strategies and structure design. *Chem Soc Rev.* **2017**, *46*, 481-558. <https://doi.org/10.1039/C6CS00829A>

71. Jin, X.; Lim, J.; Ha, Y.; Kwon, N.H.; Shin, H.; Kim, I.Y.; Lee, N-S.; Kim, M.H.; Kim, H.; Hwang, S-J. A critical role of catalyst morphology in low-temperature synthesis of carbon nanotube-transition metal oxide nanocomposite. *Nanoscale.* **2017**, *9*, 12416-12424. <https://doi.org/10.1039/C7NR03598E>

72. Aruna, S.T.; Kini, N.S.; Rajam, K.S. Solution combustion synthesis of CeO₂-CeAlO₃ nano-composites by mixture-of-fuels approach. *Mater Res Bull.* **2009**, *44*, 728-733. <https://doi.org/10.1016/j.materresbull.2008.09.034>

73. Rizwan, M.; Gul, S.; Iqbal, T.; Mushtaq, U.; Farooq, M.H.; Farman, M.; Bibi, R., Ijaz, M. A review on perovskite lanthanum aluminate (LaAlO_3), its properties and applications. *Mater Res Express*. **2019**, *6*, 112001-112031. <https://doi.org/10.1088/2053-1591/ab4629>

74. Arzeo, M.; Lombardi, F.; Bauch, T. Microwave losses in MgO , LaAlO_3 , and $(\text{La}_0.3\text{Sr}_0.7)(\text{Al}_0.65\text{Ta}_0.35)\text{O}_3$ dielectrics at low power and in the millikelvin temperature range. *Appl Phys Lett*. **2014**, *104*, 212601-212605. <https://doi.org/10.1063/1.4880357>

75. Chen, T-Y.; Pan, R-Y.; Fung, K-Z. Effect of divalent dopants on crystal structure and electrical properties of LaAlO_3 perovskite. *J Phys Chem Solids*. **2008**, *69*, 540-546. <https://doi.org/10.1016/j.jpcs.2007.07.039>

76. Sim, Y.; Yang, I.; Kwon, D.; Ha, J-M.; Jung, J.C. Preparation of LaAlO_3 perovskite catalysts by simple solid-state method for oxidative coupling of methane. *Catal Today*. **2020**, *352*, 134-139. <https://doi.org/10.1016/j.cattod.2019.10.038>

77. Lee, M-H.; Jung, W-S. Facile synthesis of LaAlO_3 and Eu (II)-doped LaAlO_3 powders by a solid-state reaction. *Ceram Int*. **2015**, *41*, 5561-5567. <https://doi.org/10.1016/j.ceramint.2014.12.133>

78. Lee, G.; Kim, I.; Yang, I.; Ha, J-M.; Na, H.B.; Jung, J.C., Effects of the preparation method on the crystallinity and catalytic activity of LaAlO_3 perovskites for oxidative coupling of methan. *Appl Surf Sci*. **2018**, *429*, 55-61. <https://doi.org/10.1016/j.apsusc.2017.08.092>

79. Yu, H-F.; Guo, Y-M. Effects of heating atmosphere on formation of crystalline citrate-derived LaAlO_3 nanoparticles. *J Alloys Compd*. **2011**, *509*, 1984-1988. <https://doi.org/10.1016/j.jallcom.2010.10.109>

80. Ianoş, R.; Borcănescu, S.; Lazău, R. Large surface area ZnAl_2O_4 powders prepared by a modified combustion technique. *Chem Eng J*. **2014**, *240*, 260-263. <https://doi.org/10.1016/j.cej.2013.11.082>

81. Patra, A.; Chandaluri, C.G.; Radhakrishnan, T. Optical materials based on molecular nanoparticles. *Nanoscale*. **2012**, *4*, 343-359. <https://doi.org/10.1039/C1NR11313E>

82. Strachowski, T.; Grzanka, E.; Mizeracki, J.; Chlenda, A.; Baran, M.; Małek, M.; Niedziałek, M. Microwave-assisted hydrothermal synthesis of zinc-aluminum spinel ZnAl_2O_4 . *Matls*. **2021**, *15*, 245-257. <https://doi.org/10.3390/ma15010245>

83. Birhi, D.N.; Laka, A.F. Study of the efficiency of ZnAl_2O_4 as green nanocatalyst. *Inornatus Biol Educ J*. **2024**, *4*, 11-26. <https://doi.org/10.30862/inornatus.v4i1.584>

84. Maity, G.; Maji, P.; Sain, S.; Das, S.; Kar, T.; Pradhan, S. Microstructure, optical and electrical characterizations of nanocrystalline ZnAl_2O_4 spinel synthesized by mechanical alloying: Effect of sintering on microstructure and properties. *Physica E Low Dimens Syst Nanostruct*. **2019**, *108*, 411-420. <https://doi.org/10.1016/j.physe.2018.10.024>

85. Han, M.; Wang, Z.; Xu, Y.; Wu, R.; Jiao, S.; Chen, Y.; Feng, S. Physical properties of MgAl_2O_4 , CoAl_2O_4 , NiAl_2O_4 , CuAl_2O_4 , and ZnAl_2O_4 spinels synthesized by a solution combustion method. *Mater Chem Phys*. **2018**, *215*, 251-258. <https://doi.org/10.1016/j.matchemphys.2018.05.029>

86. Tshabalala, K.G. Synthesis and characterization of down- conversion nanophosphors, University of the Free State, 2014.

87. Jilani, A.; Yahia, I.; Abdel-wahab, M.S.; Al-ghamdi, A.A.; Alhummiany, H. Correction to: Novel Control of the Synthesis and Band Gap of Zinc Aluminate (ZnAl_2O_4) by Using a DC/RF Sputtering Technique. *Silicon*. **2019**, *11*, 577-577. <https://doi.org/10.1007/s12633-017-9595-0>

88. Busca, G. *Structural, surface, and catalytic properties of aluminas, Advances in catalysis*, Elsevier. 2014; pp 319-404. <https://doi.org/10.1016/B978-0-12-800127-1.00003-5>

89. Nikoofar, K.; Shahedi, Y.; Chenarboor, F.J. Nano alumina catalytic applications in organic transformations. *Mini-Rev Org Chem*. **2019**, *16*, 102-110. <https://doi.org/10.2174/1570193X15666180529122805>

90. Kazemi, H.; Kermani, F.; Mollazadeh, S.; Vahdati Khakhi, J. The significant role of the glycine-nitrate ratio on the physicochemical properties of $\text{CoxZn}_{1-x}\text{O}$ nanoparticles. *Int J Appl Ceram Technol*. **2020**, *17*, 1852-1868. <https://doi.org/10.1111/ijac.13515>

91. Cai, W.; Zhang, S.; Lv, J.; Chen, J.; Yang, J.; Wang, Y.; Guo, X.; Peng, L.; Ding, W.; Chen, Y. Nanotubular gamma alumina with high-energy external surfaces: synthesis and high performance for catalysis. *ACS Catal*. **2017**, *7*, 4083-4092. <https://doi.org/10.1021/acscatal.7b00080>

92. Eliassi, A.; Ranjbar, M. Application of novel gamma alumina nano structure for preparation of dimethyl ether from methanol. *Int j nanosci nanotechnol*. **2014**, *10*, 13-26.

93. Paranjpe, K.Y. Alpha, beta and gamma alumina as a catalyst-A Review. *Pharma Innov J.* **2017**, *6*, 236-238.

94. Sherikar, B.N.; Sahoo, B.; Umarji, A.M. Effect of fuel and fuel to oxidizer ratio in solution combustion synthesis of nanoceramic powders: MgO, CaO and ZnO. *Solid State Sci.* **2020**, *109*, 106426-106434. <https://doi.org/10.1016/j.solidstatesciences.2020.106426>

95. Behera, P.; Sarkar, R.; Bhattacharyya, S. Nano alumina: a review of the powder synthesis method. *InterCeram: Int Ceram Rev.* **2016**, *65*, 10-16. <https://doi.org/10.1007/BF03401148>

96. Sharma, A.; Rani, A.; Singh, A.; Modi, O.; Gupta, G.K. Synthesis of alumina powder by the urea-glycine-nitrate combustion process: a mixed fuel approach to nanoscale metal oxides. *Appl Nanosci.* **2014**, *4*, 315-323. <https://doi.org/10.1007/s13204-013-0199-8>

97. Khaliullin, S.M.; Zhuravlev, V.D.; Bamburov, V.G. Solution-combustion synthesis of oxide nanoparticles from nitrate solutions containing glycine and urea: Thermodynamic aspects. *Int J Self-Propagating High-Temp Synth.* **2016**, *25*, 139-148. <https://doi.org/10.1016/B978-0-12-804173-4.00079-X>

98. Patil, K.C.; Aruna, S.T.; Mimani, T. Combustion synthesis: an update. *Curr Opin Solid State Mater Sci.* **2002**, *6*, 507-512. [https://doi.org/10.1016/S1359-0286\(02\)00123-7](https://doi.org/10.1016/S1359-0286(02)00123-7)

99. Goworek, J.; Kierys, A.; Gac, W.; Borowka, A.; Kusak, R. Thermal degradation of CTAB in as-synthesized MCM-41. *J Therm Anal Calorim.* **2009**, *96*, 375-382. <https://doi.org/10.1007/s10973-008-9055-6>

100. Mandal, K.; Ghose, S.; Mandal, M.; Majumder, D.; Talukdar, S.; Chakraborty, I.; Panda, S.K. Notes on useful materials and synthesis through various chemical solution techniques, Chemical Solution Synthesis for Materials Design and Thin Film Device Applications, Elsevier. 2021; pp 29-78. <https://doi.org/10.1016/B978-0-12-819718-9.00011-X>

101. Shukla, R.; Dutta, D.P.; Ramkumar, J.; Mandal, B.P.; Tyagi, A.K. Nanocrystalline Functional Oxide Materials. *Springer Handbook of Nanomaterials.* **2013**, 517-552. https://doi.org/10.1007/978-3-642-20595-8_13

102. Lazarova, T.; Kovacheva, D.; Cherkezova-Zheleva, Z.; Tyuliev, G. Studies of the possibilities to obtain nanosized MnFe₂O₄ by solution combustion synthesis. *Bulg Chem Commun.* **2017**, *49*, 217-224. WOS:000418322200039

103. Evdokimenko, N.; Yermekova, Z.; Roslyakov, S.; Tkachenko, O.; Kapustin, G.; Bindiug, D.; Kustov, A.; Mukasyan, A.S. Sponge-like CoNi catalysts synthesized by combustion of reactive solutions: Stability and performance for CO₂ hydrogenation. *Matls.* **2022**, *15*, 5129-5147. <https://doi.org/10.3390/ma15155129>

104. Meza-Trujillo, I.; Devred, F.; Gaigneaux, E.M. Production of high surface area mayenite (C12A7) via an assisted solution combustion synthesis (SCS) toward catalytic soot oxidation. *Mater Res Bull.* **2019**, *119*, 110542-110551. <https://doi.org/10.1016/j.materresbull.2019.110542>

105. Meza-Trujillo, I.; Mary, A.; Pietrzyk, P.; Sojka, Z.; Gaigneaux, E.M. Nature and role of Cu (II) species in doped C12A7 catalysts for soot oxidation. *Appl Catal B: Environ.* **2022**, *316*, 121604-121618. <https://doi.org/10.1016/j.apcatb.2022.121604>

106. Lutukurthi, D.N.V.V.K.; Dutta, S.; Behara, D.K. Dual role of activated carbon as fuel and template for solution combustion synthesis of porous zinc oxide powders. *J Am Ceram Soc.* **2021**, *104*, 4624-4636. <https://doi.org/10.1111/jace.17841>

107. Paborji, F.; Afarani, M.S.; Arabi, A.M.; Ghahari, M. Synthesis of (Fe, Cr) 2O₃ solid solution pigment powders for ink application. *Int J Appl Ceram Technol.* **2023**, *20*, 1154-1166. <https://doi.org/10.1111/ijac.14263>

108. Paborji, F.; Shafiee Afarani, M.; Arabi, A.M.; Ghahari, M. Phase transformation of FeCr₂O₄ to (Fe, Cr) 2O₃ solid solution pigment powders: Effect of post-heating temperature. *Int J Appl Ceram Technol.* **2023**, *20*, 281-293. <https://doi.org/10.1111/ijac.14189>

Disclaimer/Publisher's Note: The statements, opinions and data contained in all publications are solely those of the individual author(s) and contributor(s) and not of MDPI and/or the editor(s). MDPI and/or the editor(s) disclaim responsibility for any injury to people or property resulting from any ideas, methods, instructions or products referred to in the content.